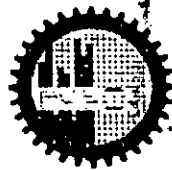
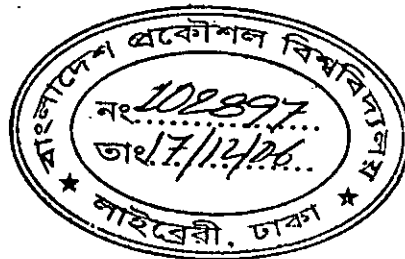


# Thermal Stress Analysis of Side-Hole Optical Fibers with Elliptical Core

Md. Ashraful Islam



BUET



DEPARTMENT OF ELECTRICAL AND ELECTRONIC ENGINEERING  
BANGLADESH UNIVERSITY OF ENGINEERING AND TECHNOLOGY

May 2006

# **Thermal Stress Analysis of Side-Hole Optical Fibers with Elliptical Core**

By  
**Md. Ashraful Islam**


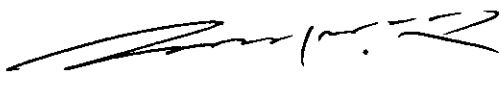
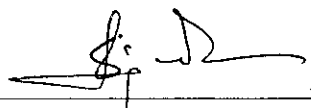

A thesis submitted to the Department of Electrical and Electronic Engineering of Bangladesh University of Engineering and Technology (BUET) in partial fulfillment of the requirements for the degree of  
**Master of Science in Electrical and Electronic Engineering**



**DEPARTMENT OF ELECTRICAL AND ELECTRONIC ENGINEERING  
BANGLADESH UNIVERSITY OF ENGINEERING AND TECHNOLOGY  
May 2006**

The thesis entitled “**Thermal Stress Analysis of Side-Hole Optical Fibers with Elliptical Core**” submitted by Md. Ashraful Islam, Roll No. 040206254F, Session. April, 2002 has been accepted as satisfactory in partial fulfillment of the requirement for the degree of **Master of Science in Electrical and Electronic Engineering on the date of 27/05/2006.**

**BOARD OF EXAMINERS**

1.  27/5/06  
\_\_\_\_\_  
**Dr. Md. Shah Alam**  
Associate Professor  
Department of Electrical and Electronic Engineering  
BUET, Dhaka-1000, Bangladesh  
**Chairman**  
(Supervisor)
2.   
\_\_\_\_\_  
**Dr. S. Shahnawaz Ahmed**  
Professor and Head  
Department of Electrical and Electronic Engineering  
BUET, Dhaka-1000, Bangladesh  
**Member**  
(Ex-Officio)
3.  27/5/06  
\_\_\_\_\_  
**Dr. Satya Prasad Majumder**  
Professor  
Department of Electrical and Electronic Engineering  
BUET, Dhaka-1000, Bangladesh  
**Member**
4.  27.5.06  
\_\_\_\_\_  
**Dr. Md. Nazrul Islam**  
Associate Professor  
Department of Physics  
BUET, Dhaka-1000, Bangladesh  
**Member**  
(External)

# Declaration

It is hereby declared that this thesis or any part of it has not been submitted elsewhere for the award of any degree or diploma.

A handwritten signature in black ink, appearing to read 'Ashraful', is written over a horizontal line.

Signature of the candidate  
(Md. Ashraful Islam)

# Dedication

*To my beloved parents, sisters and brothers.*

# Table of Contents

<b>Declaration</b>		<b>iv</b>
<b>Dedication</b>		<b>v</b>
<b>List of abbreviations</b>		<b>viii</b>
<b>List of symbols</b>		<b>ix</b>
<b>List of Figures</b>		<b>x</b>
<b>Acknowledgements</b>		<b>xiii</b>
<b>Abstract</b>		<b>xiv</b>
<b>1</b>	<b>Introduction</b> ...    ...    ...    ...    ...    ...    ...    ...    ...	<b>1</b>
1.1	Literature Review .....	1
1.2	Objective of the work .....	3
1.3	Layout of the thesis .....	3
<b>2</b>	<b>The Optical fibers</b> ...    ...    ...    ...    ...    ...    ...    ...	<b>5</b>
2.1	The Mechanism of Light Propagation in Optical Fibers .....	6
2.2	Classification of Optical Fiber .....	8
2.3	Polarization Maintaining Fiber .....	10
2.3.1	PMF with Side-Pits and Side Tunnels.....	11
2.3.2	PMF with Stress Induced Parts .....	12
2.3.3	PMF with Geometrical Asymmetry .....	13
2.4	Polarization Mode Dispersion and The Effect of Birefringence .....	14
<b>3</b>	<b>Finite Element Method</b> ...    ...    ...    ...    ...    ...    ...	<b>15</b>
3.1	Boundary value problems .....	17
3.2	Basic steps of the finite element method .....	17
3.2.1	Domain Discretization .....	18
3.2.2	Selection of the interpolation functions .....	22
3.2.3	Formulation of the System of Equations .....	24
3.2.4	Solution of the System of Equations .....	28

<b>4</b>	<b>Stress Analysis of Optical Fiber</b>	...	...	...	...	...	...	<b>30</b>
4.1	Introduction	.....						30
4.2	Energy Principle	.....						30
4.3	Stresses and strain in optical fibers	.....						31
4.4	Mathematical Formulation	.....						33
<b>5</b>	<b>Numerical Results and Discussion</b>	...	...	...	...	...	...	<b>41</b>
5.1	Structure of the system	.....						41
5.2	Results and Discussions	.....						43
5.3	Results of Side-hole Fiber with Elliptical Core	.....						52
<b>6</b>	<b>Conclusions</b>	...	...	...	...	...	...	<b>60</b>
6.1	Summary of the work	.....						60
6.2	Future research scope	.....						61
	<b>References</b>	...	...	...	...	...	...	<b>62</b>

# List of Abbreviations

<b>PM</b>	Polarization maintaining
<b>PMF</b>	Polarization maintaining fiber
<b>FEM</b>	Finite element method
<b>FEA</b>	Finite element analysis
<b>SAP</b>	Stress applying part
<b>PANDA</b>	Polarization maintaining and absorption reducing fiber
<b>MCVD</b>	Modified chemical vapor deposition



# List of Symbols

$\Omega$	Domain
$L$	Differential operator
$f$	Excitation or forcing function
$\phi$	Scalar potential
$\varepsilon$	Permittivity of medium
$\rho$	Electric charge density
$S$	Domain to be descritized according to FEM
$M$	Total number of sub-domains
$n(i, e)$	Connectivity Array for sub-domain numbering
$a^e, b^e$ and $c^e$	Constant coefficient
$e$	Number of element
$n$	Number of nodes in the element
$N_j^e$	Interpolation function
$j$	Node number
$\Delta$	Area of an element
$\Pi$	Total potential energy
$U$	Strain energy
$V$	Work done by the external force
$\varepsilon_x, \varepsilon_y,$ and $\varepsilon_z$	Spatial variations of the principal strains along the $x$ -, $y$ -, and $z$ -axis directions, respectively
$\gamma_{xy}$	Shear strain in the $x$ - $y$ plane
$\sigma_x, \sigma_y,$ and $\sigma_z$	Spatial variations of the principal stresses along the $x$ -, $y$ -, and $z$ -axis directions, respectively
$\tau_{xy}$	Shear stress in the $x$ - $y$ plane
$G$	M modulus of rigidity

# List of Figures

2.1	Optical fiber wave guide .....	6
2.2	Refraction of light .....	6
2.3	Light transmission through fiber .....	7
2.4	(a) Single mode fiber, (b) Multimode fiber.....	8
2.5	Refractive index profile and ray transmission in (a) step index fiber, (b) graded index fiber .....	9
2.6	Side-pit Fiber. (a) Cross section, (b) Refractive index distribution .....	12
2.7	Cross section of PMF. (a) Bow-tie fiber, and (b) PANDA fiber .....	12
2.8	Fiber cross section (a) Elliptical core with circular clad, (b) Circular core with elliptical clad .....	13
3.1	Subdivision of structure into small element .....	16
3.2	Basic finite elements. (a) One dimensional, (b) Two dimensional, and (c) Three dimensional .....	18
3.3	(a) Finite element division of optical fiber. (b) Linear triangular elements..	20
3.4	Subdivision of a two dimensional domain .....	21
3.5	Linear interpolation functions for a triangular element. (a) $N_1^e$ , (b) $N_2^e$ and (c) $N_3^e$ .....	24
5.1	(a) Cross section of a circular core fiber, (b) Comparison of thermal stress obtained from analytical method and the FEM method .....	44
5.2	Stress ( $\sigma_x$ ) distribution over the cross section of circular fiber .....	45
5.3	Contour map corresponding to Fig. 5.2 .....	45
5.4	Stress ( $\sigma_y$ ) distribution over the cross section of circular fiber .....	46
5.5	Contour map corresponding to Fig. 5.4 .....	46
5.6	Cross section of an elliptical core fiber .....	47
5.7	Variation of birefringence with core ellipticity .....	47
5.8	Stress ( $\sigma_x$ ) distribution over the cross section of elliptical core ( $\epsilon = 0.6$ ) fiber .....	49

5.9	Contour map corresponding to Fig. 5.8	49
5.10	Stress ( $\sigma_y$ ) distribution over the cross section of elliptical core ( $\epsilon = 0.6$ ) fiber	50
5.11	Contour map corresponding to Fig. 5.10	50
5.12	Refractive index difference ( $\Delta n_x$ ) and the corresponding contour map over the cross section of elliptical core ( $\epsilon = 0.6$ ) fiber	51
5.13	Refractive index difference ( $\Delta n_y$ ) and the corresponding contour map over the cross section of elliptical core ( $\epsilon = 0.6$ ) fiber	51
5.14	Cross section of the side-hole fiber with elliptical core	52
5.15	Birefringence versus pitch length of side-hole fiber	52
5.16	Birefringence versus pitch length when core ellipticity, $\epsilon = 0.6$	53
5.17	Birefringence versus pitch length with core ellipticity, $\epsilon = 0.6$ and $0.5$	53
5.18	The birefringence versus thermal expansion co-efficient of fiber core material	54
5.19	Birefringence versus air hole radius for a pitch length, $\Gamma = 20.0 \mu\text{m}$	55
5.20	Birefringence versus air-hole radius for different pitch length when core ellipticity, $\epsilon = 0.6$	55
5.21	Birefringence versus air-hole radius for different core radius with pitch length $30 \mu\text{m}$ and core ellipticity $0.6$	56
5.22	Change of refractive index ( $n_x$ ) over the cross section for circular core side hole fiber with $\Gamma = 20.0 \mu\text{m}$ and $r = 7.5 \mu\text{m}$	57
5.23	5.23: Contour map corresponding to Fig.5.22	57
5.24	Change of refractive index ( $n_y$ ) over the cross section for circular core side hole fiber with $\Gamma = 20.0 \mu\text{m}$ and $r = 7.5 \mu\text{m}$	58
5.25	Contour map corresponding to Fig. 5.24	58

# List of Tables

- 3.1 Numbering arrangement for global number, local number and element number.. 21

# Acknowledgements

I would like to convey my heartiest gratitude and profound respect to my supervisor Dr. Md. Shah Alam, Associate Professor, Department of Electrical and Electronic Engineering, Bangladesh University of Engineering and Technology (BUET), Dhaka, for his continuous guidance, constructive suggestions, critical remarks and wholehearted supervision throughout the progress of this work. Without his valuable direction and cordial assistant this study would never be materialized. I am deeply indebted to him for acquainting me with the world of advanced research.

I am grateful to the Head of the Department of EEE, BUET to make all the research facilities of the department accessible to me. I would also like to extend my thanks to the authority of Bangladesh Public Works Department (BPWD) for giving me the opportunity to continue this research study. I also thank to Ms. Anisa Begum, Head and Principal Engineer, Electronics Division of Atomic Energy Centre, Dhaka, for her continuous inspiration towards this work.

The author would like to thank his friends, colleagues and well wishers who extended their helping hands directly or indirectly regarding this study. Finally, I am grateful to Almighty Allah for giving me strength and courage to complete the work.

# Abstract

A thermal stress analysis of side-hole optical fiber with elliptical core has been presented in this work by using a finite element method. The birefringence because of the thermal stress, which is caused in the structure due to the different thermal expansion coefficients of core and cladding and also the geometrical birefringence are simultaneously considered here in this work. The analysis here is based on the plain strain approximation and potential energy principle in the finite element method, which in this case, results in a linear system of unknown displacements at the nodes. After checking the accuracy of finite-element calculations, thermal stress analysis of elliptical cored fibers and side hole fibers with elliptical core are performed. The influences of core ellipticity, air hole radius and position, as well as the thermal expansion coefficient of core and cladding materials on fiber birefringence are systematically assessed. Also, the work is further extended to calculate the changed refractive index in  $x$  and  $y$  polarized light due to photo-elastic effect.

For a fiber with elliptical core, the birefringence increases with the core ellipticity as the stress in and around the core gets higher with the increase in the core ellipticity. Fiber birefringence increases with larger pitch length. Thus, fiber with higher core ellipticity and higher pitch length generates higher birefringence. On the other hand, the birefringence decreases with the increase in side-hole radius. Smaller side-holes can produce moderately higher birefringence if they are far from the core. Thus, the simulation results suggest that, elliptical core side-hole fiber can be treated as a good candidate for *high birefringent* polarization maintaining fiber (PMF), which finds increasing demands in coherent optical communication, optical fiber sensing devices and many other applications.



## Chapter 1

# Introduction

In ordinary single-mode fibers widely used in present optical communication systems, the polarization states of the input and the output light beams do not match, since the polarization of the output light beam is unstable. By contrast, the polarization maintaining (PM) fibers maintain the state of polarization of a light beam passing through them. PM fibers are imperative for obtaining a stable output in interferometric fiber optical sensors. In optical communication devices the use of PM fiber becomes mandatory when performing any polarized waves operations; e.g., for polarization combining. There are many applications where the polarization of the light is required to be stable and well defined such as coupling to the integrated optical circuits, interferometric sensors, coherent optical communication systems, and certain in-line fiber optic components. So, it is very important to study the polarization state of a fiber when it is designed for a communication system. In this work a PM fiber called the side-hole fiber will be studied using a thermal stress analysis using the finite element method (FEM). Before we go into details, first in this chapter we review the literature with regard to the thermal stress analysis of fiber and then mention the motivation of this work. At the end of this chapter, we also show the structure of the thesis.

### 1.1 Literature Review

Polarization maintaining fibers (PMFs) that can maintain a state of polarization over a long length are desirable for use in coherent optical communications and fiber optic sensing systems [1]-[4]. These PMFs are usually divided into two groups. One is the

axially nonsymmetrical (having elliptical core), mainly using geometrical birefringence [2], [3]-[4], and the other is the stress-applied type (fabricated with stress applied zone, SAZ), using stress-induced birefringence, *e.g.*, PANDA fiber, bowtie fiber, *etc.* [1]-[2]. Side-hole optical fibers are very similar to the PANDA fiber, but with two air-holes running along the length in place of the stress applying zones [5]-[6]. This type of fiber can exhibit large birefringence and is a good candidate as a PMF in optical fiber communication systems and also in fiber optic sensing systems [5]-[6]. This fiber introduces high birefringence because of its geometry and different thermal expansion coefficients of core and cladding materials. Because of the presence of air holes, index contrast is increased; hence modal confinement is enhanced with a reduction of optical loss [5]-[6]. This birefringence can further be increased by introducing elliptical core with circular air holes in the structure. So, in order to realize single mode operations with the side-hole fiber, a detailed analysis is necessary. As a first step, this work is motivated to the stress analysis and finding the birefringence due to the geometry and thermal stress in the fiber. While the thermal stress induced birefringence properties and dispersion are studied for widely used PMFs, *e.g.*, PANDA fiber, bowtie fiber, *etc.* [1]-[4], [7]-[9], little work has been done on side-hole optical fibers [5]-[6].

Different methods have been used to analyze various types of polarization maintaining fibers. The finite element method was used by Okoshi et al. [10]-[11] for performance analysis of side-tunnel type fiber. An H-field finite-element method was used by Hayata and co-workers [12] and the effective-index method was used in [13]. A single-mode fiber with asymmetrical refractive index pits on both sides of the core was fabricated by the MCVD method [14]. From the experimental measurement, the beat length was found to be about 23 mm and a birefringence  $B = 5 \times 10^{-5}$  was obtained. Stress analysis of a side pit fiber by the finite element method [15]-[16] shows that the contribution of the stress-induced birefringence to modal birefringence is much larger than that of the geometrical anisotropy [10]. For stress induced PMF a finite element method [15], and an analytical method [16]-[17] have been used to calculate the stress distribution due to SAPs in these fibers. It has been shown that placing the SAPs close to the core improves the birefringence of these fibers, however



in our work we investigate the birefringence property using finite element method by placing circular air hole in place of SAPs with elliptical core at the center.

## 1.2 Objective of the work

The main objective of this work is to perform the thermal stress analysis of polarization maintaining fiber, particularly for the side-hole optical fiber with elliptical core. The fiber birefringence properties induced by thermal stress will be calculated and studied. The influence of core shape and size, as well as the side-hole size and position on fiber birefringence will also be investigated. Initially we evaluate the birefringence for a simple fiber structure i.e., conventional single mode step index fiber under thermal stress; this is done for the purposes of providing the validity of the simulation program. Later, this program is further extended to calculate the birefringence for side-hole fiber with elliptical core. We also examined the effect of temperature change during fiber manufacturing and the thermal expansion coefficient of core material on the birefringence. Finally the refractive index profiles along the radial distance of various fiber structures are investigated. In this thesis work finite element method (FEM) [7]-[8] is used for the thermal stress analysis of different fiber structure. The FEM is a versatile method for handling arbitrary cross section with complex geometry. In this method, a simultaneous linear system of equations is formulated with nodal displacements as unknowns by using plane-strain approximation. The system of equations is then numerically solved using Gaussian elimination technique. For efficient solution of the problem, only one-fourth of the cross section is being discretized into linear triangular elements using the two-fold symmetry of the structure and applying the appropriate *Dirichlet* type boundary conditions on the plane of symmetry. Once the system of equation is solved for nodal displacements, it is easy to find the stress developed in each element in the cross sectional domain.

## 1.3 Layout of the Thesis

There are six chapters in this thesis. Chapter 1 presents an introduction of the work with a brief review of literature and objective of the work. Chapter 2 presents an overview of optical fiber, light propagation mechanism through it and classification of

optical fiber. Different types of polarization maintaining fibers are also discussed in this chapter.

In chapter 3, a brief and general discussion on finite element analysis (FEA), a versatile method for handling arbitrary cross section with complex geometry is presented. It also includes descriptions of various steps and corresponding mathematical formulation involved in FEA.

Chapter 4 deals with principle and computational technique used for thermal stress analysis of the fiber. Sequential formulation to calculate the fiber birefringence and changed refractive index due to thermal stress are also shown in this chapter.

Chapter 5 presents the results and discussions of this study. The results given here are for elliptical core fiber and side-hole fiber with elliptical core. A comparison between the existing results and the present results is given. Surface plots and contour maps for various fiber structures are also shown here. A short description of the developed simulation program is presented in this chapter.

Concluding remarks of this thesis work along with suggestions for future research are hosted in chapter 6.

## Chapter 2

# The Optical Fibers

Mankind has always throughout its history had the necessity for communication. Initially communication was done through signals, voice or primitive forms of writing. As time passed by there was a need to communicate through distances, to pass information from one place to another. Many different ways to exchange information have been used throughout history. Progressing from the copper wire of a century ago to today's fiber optic, our increasing ability to transmit more information, more quickly and over longer distances has expanded the boundaries of our technological development in all areas. Now a day optical fiber is being using as the backbone component in long distance and high bit-rate optical communication and networking system. Optical fibers also find important applications in a variety of sensors, communications systems, and telecommunications networks. The choice of fiber depends on where and how it is applied and what one kind of fiber can offer over the other. In particular, polarization maintaining (PM) fibers are desirable for use in optical fiber sensing and coherent long distance optical communication systems [1]. Following fundamental attractive features have made tremendous use and demand of optical fiber:

- Enormous potential bandwidth ( $\sim 10^{14}$  Hz).
- Immunity from electromagnetic interference.
- Low transmission loss ( 0.2dB/km).
- Reliability i.e, security of the signal.
- Potential low cost.
- Small size and light in weight.

## 2.1 The Mechanism of Light Propagation in Optical Fibers

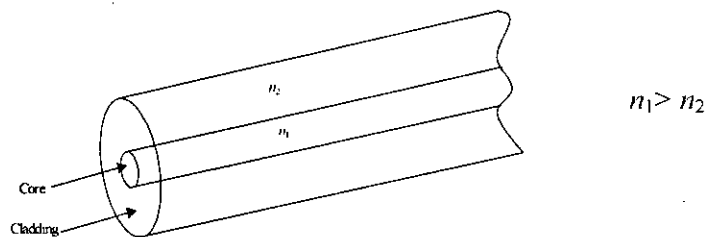


Fig. 2.1: Optical fiber waveguide.

An optical fiber is a circular waveguide that takes the form of a long, thin strand of glass about the diameter of a human hair. This fiber contains two concentric glass regions with slightly different refractive indices. The refractive index is the ratio of the speed of light in a vacuum to its speed in the glass fiber medium. The center of the fiber through which most of the light travels is called the fiber core. The outer region, having a lower refractive index than the inner region, is called the cladding. A surrounding plastic coating is used to protect the glass fiber. Additionally, an encasing cable structure is often applied to protect the optical fiber during installation and operation.

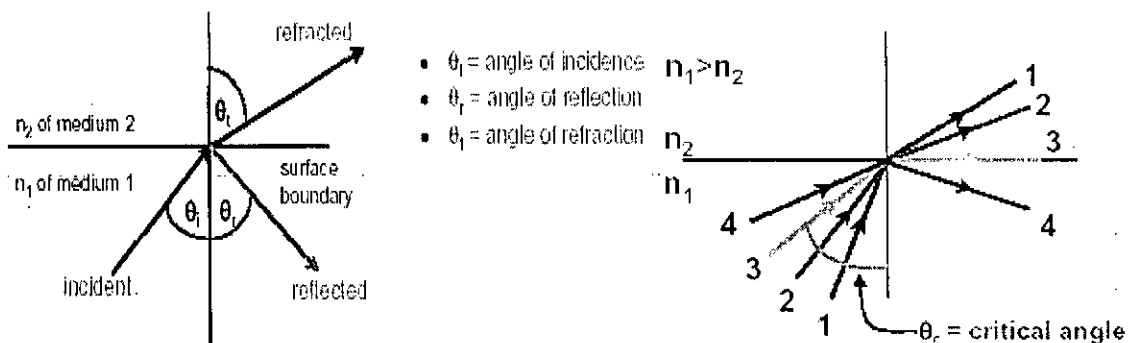


Fig. 2.2: Refraction of light.

The propagation of light within an optical fiber can be well understood using ray model theory. According to the ray theory, when a light ray is incident on the interface between two dielectrics of different refractive indices some of the light

refracts, some reflects and other is absorbed as illustrated in Fig. 2.2. The amount of refraction, reflection and absorption depend on two dielectrics and the interface. If the incident angle is such that the refraction angle is  $90^\circ$ , i.e, the refracted ray emerges parallel to the interface then the incident angle is known as critical angle  $\theta_c$ . When the incident angle is greater than the critical angle then all the light reflects back to the first medium or dielectric and this phenomenon is known as total internal reflection [18].

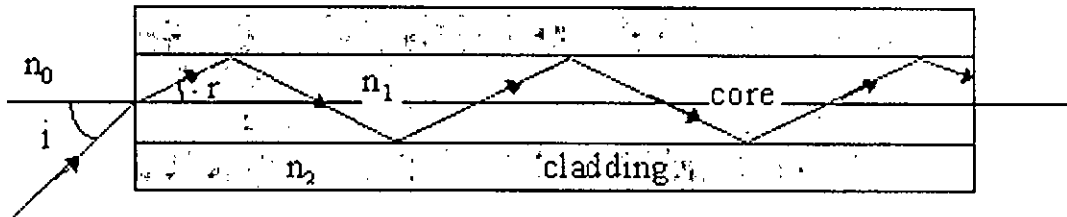


Fig. 2.3: Light transmission through fiber.

In optical fiber the light is launched into the entrance face of the fiber and is propagated by the total internal reflection at the interface between core and cladding. However the rays incident at angles larger than a certain angle, called the cut-off angle, suffer both refraction and reflection at the interface between the core and the cladding. Therefore, they are not guided. Due to this the optical fiber has a numerical aperture. The numerical aperture is given by the square root of  $(n_1^2 - n_2^2)$ . Typical values of numerical aperture lie between 0.1 and 0.3.

Consider the Fig. 2.3, which is a section of the optical fiber. The refractive indices of the core and the cladding are  $n_1$  and  $n_2$  respectively. Suppose the fiber is in air ( $n_0=1$ ). The axis of the cylindrical structure is the optical axis. When a ray is incident with an angle  $i$  at the entrance face, it is refracted into the core. Then it strikes the core-cladding interface at a certain angle. If this angle exceeds the critical angle, it is totally reflected and strikes the interface on the other side of the axis. Here it is again totally reflected using the same phenomena. This process is repeated till the ray emerges out of the fiber at the other end. The ray is thus guided by total internal reflection.

The angle of incidence at the entrance face for which the ray strikes the core-cladding interface at the critical angle is called the cut-off angle. The ray is guided for all the angles of incidence smaller than the cut-off angle at the entrance face. Also the numerical aperture is equal to  $n_0$  times the sine of cut-off angle. However, if the angle of incidence at the interface is less than the critical angle, both reflection and refraction takes place. Due to refraction at each incidence on the interface, the light beam dies off over a certain distance. There is no guidance.

## 2.2 Classification of Optical Fibers

Optical fiber can be classified from various point of views.

- In terms of physical dimension optical fibers are of two types:

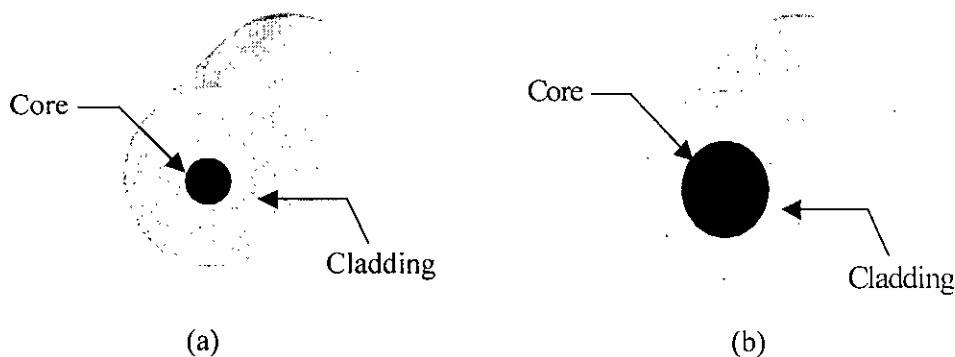


Fig. 2.4: (a) Single mode fiber. (b) Multi-mode fiber.

**Single mode fiber:** Single mode fiber is the fiber that allows only one transverse electromagnetic mode to propagate. Typically it has the core diameter of 2-10  $\mu\text{m}$  [19]. It has the distinct advantage of low intermodal dispersion and is generally used for low loss signal transmission and high speed long distance communication.

**Multi-mode fiber:** In multi-mode fiber a finite number of guided modes are allowed to propagate through the channel. The number of guides modes depends on the physical parameters (i.e. core radius, refractive index difference) of the fiber and the wavelength of the transmitted light. Generally it has the core diameter of 50 - 100  $\mu\text{m}$ . Although it offers considerable dispersion loss, it facilitates easier coupling with

less tolerance requirements and very useful with incoherent optical sources [20]-[21]. It is better suited for shorter distance communication.

- From refractive index profile (of the core) point of view, fibers are of two kinds:

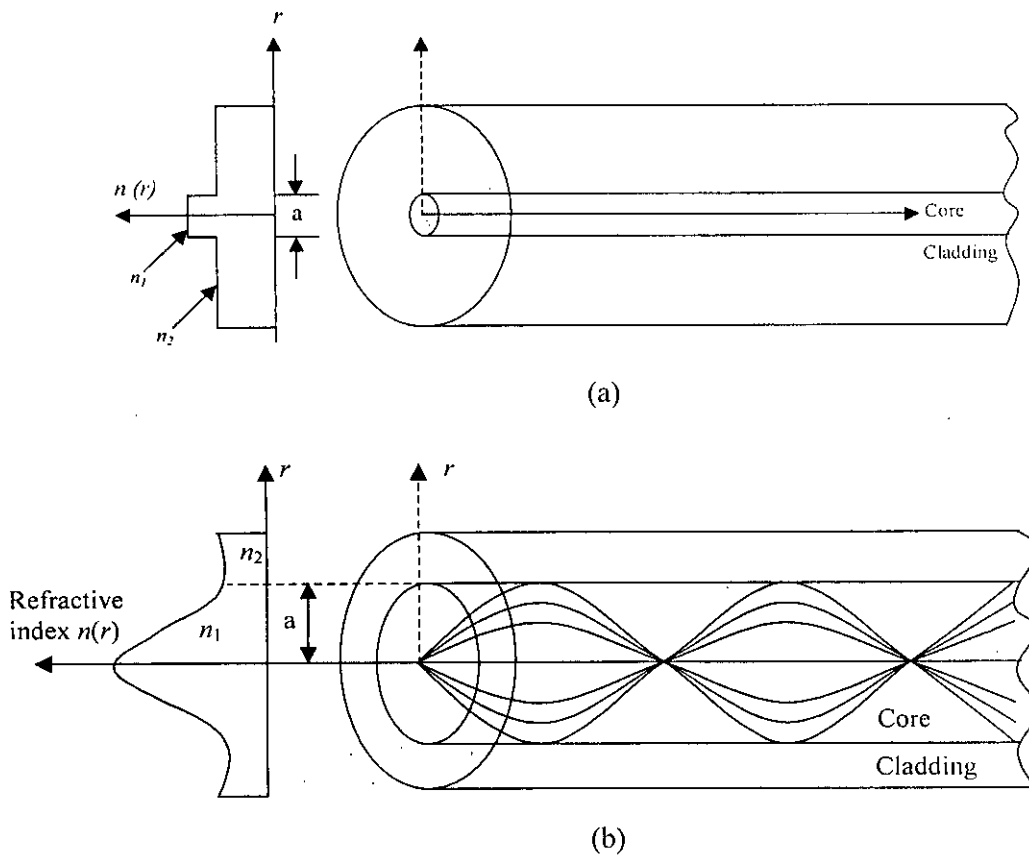


Fig. 2.5: The refractive index profile and ray transmission. (a) Step index fiber.  
(b) Graded index fiber.

**Step index fiber:** Step index fiber is a kind of fiber where the refractive index of core is maintained at a fixed value (say  $n_1$ ) and that of cladding is continued at a slightly lower refractive index (say  $n_2$ ) i.e.  $n_1 > n_2$  as shown in the Fig. 2.5 (a). Since the refractive index profile changes in step at the core-cladding interface hence the name is step index fiber.

**Graded index fiber:** Graded index fibers do not have a constant refractive index in the core, rather have a decreasing core index  $n(r)$  with radial distance from a maximum value of  $n_1$  at the axis to a constant value  $n_2$  beyond the core radius  $a$  in the cladding is as shown in the Fig. 2.5(b). This index variation may be represented as [19]:

$$n(r) = \begin{cases} n_1(1 - 2\Delta(r/a)^\alpha)^{1/2} & r < a \text{ (core)} \\ n_1(1 - 2\Delta)^{1/2} = n_2 & r \geq a \text{ (cladding)} \end{cases}$$

where  $\Delta$  is the refractive index difference and  $\alpha$  is the profile parameter of core refractive index characteristic. For  $\alpha=1$ , core index profile is triangular and for  $\alpha=2$ , core index profile is parabolic.

### 2.3 Polarization Maintaining Fiber

Shortly after the introduction of single mode fiber, it became evident that linear polarization states were not preserved in long fiber lengths. This is due to perturbing birefringence resulting from either internal defects such as the nonideal geometry of the core and cladding or externally applied bends, twists, squeeze, clamps, etc. to the fiber. This effect causes a change in the polarization state of light propagating in the fiber. These problems motivated the development of a special kind of fibers named as *polarization maintaining fiber*, which is not a fiber without birefringence, but to the contrary a fiber with a strong built-in birefringence. In these fibers the polarization of light launched into the fiber is aligned with one of the birefringent axes and this polarization state will be preserved even if the fiber is bent [1],[22].

The polarization of wave describes the time varying behavior of the electric field vector at a fixed point in space. Polarization is observed along the direction of propagation by tracing out the tip of the instantaneous electric field. There are three types of wave polarization: linear, circular, and elliptical. In general, the tip of the electric field vector traces out an ellipse and the wave is said to be elliptically polarized. The other two types of polarization, linear and circular, are special cases of elliptical polarization. The linearly polarized wave is characterized by the property that the orientation of the electric field vector is the same everywhere in space and is



independent of time [23]. In linear polarization, the field vector is directed along a line. The circularly polarized wave is characterized by a constant amplitude field vector, and the field vector orientation in space changes continuously with time so that the tip of the field vector traces out a circular locus in a plane transverse to the direction of propagation.

There are mainly two kinds of PM fibers. One kind is the axially nonsymmetrical using geometrical birefringence, such as the elliptical core fiber or the D-shaped cladding fiber. The core or the cladding of this kind of fiber is normally deformed from a circular shape so as to generate an anisotropy of the fiber structure. The other kind is stress-applied type using stress-induced birefringence, such as PANDA fiber or bow-tie fiber. Here the birefringence is induced due to elasto-optic effect [1]. Side-hole fiber is very similar to PANDA fiber, but in contrast of having stress applying zone it has two air holes running along the fiber axis. This type of fiber can exhibit large birefringence and is a good candidate as PM fiber. This fiber introduces high birefringence because of its geometry and different thermal expansion coefficients of core and cladding materials [24]-[25].

A commonly used method to introduce strong birefringence is to include two stress rods of a modified glass composition in the preform on opposite sides of the core. When a fiber is drawn from such a preform, the stress rods cause some stress with a well defined orientation. Another technique is to use an elliptical core. In any case, the birefringent beat length can be so small (few millimeters) that additional stress effects are too weak to cause significant mixing of the polarization states.

### 2.3.1 PMF with Side-Pits and Side Tunnels

Side-pit fibers as shown in Fig. 2.6 incorporate two pits of refractive index  $n_p$  less than the cladding index  $n_{cd}$ , on each side of the central core. This type of single polarization fiber was first proposed by Okoshi and Oyamada [26]. It has a W-type index profile along the  $x$ -axis and a step index profile along the  $y$ -axis. A side-tunnel fiber is a special case of side-pit structure when the two pits are hollow with  $n_p = 1$ . In these fibers, a geometrical anisotropy is introduced in the core to obtain a birefringent fiber.

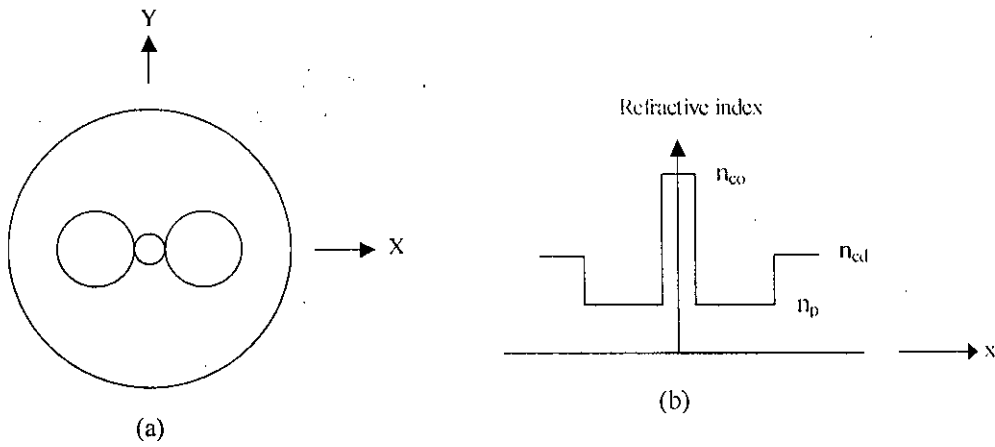


Fig. 2.6: Side-pit Fiber. (a) Cross section. (b) Refractive index distribution.

### 2.3.2 PMF with Stress Induced Parts

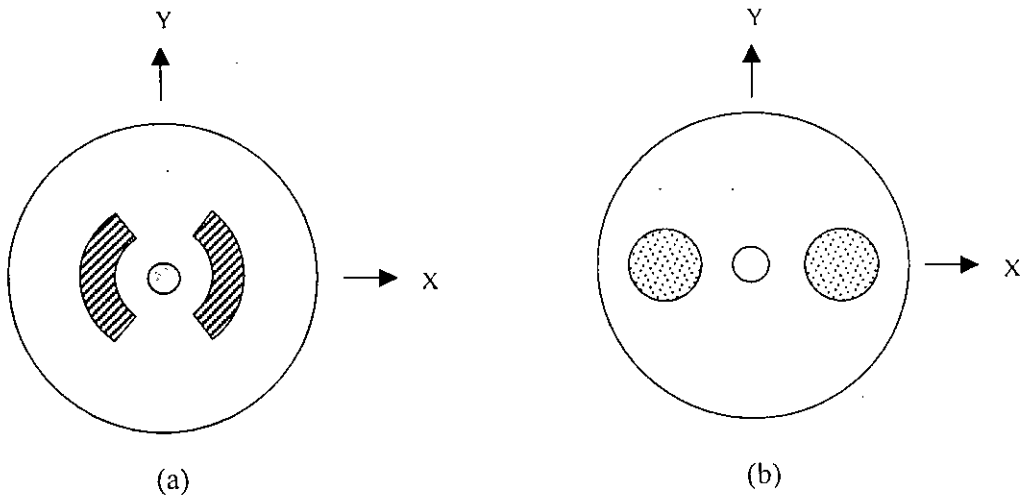


Fig. 2.7: Cross section of PMF. (a) Bow-tie fiber, and (b) PANDA fiber.

An effective method of introducing high birefringence in optical fibers is by introducing an asymmetric stress, with two-fold geometrical symmetry in the core of the fiber. The stress changes the refractive index of the core due to photoelastic effect, seen by the modes polarized along the principal axes of the fiber, and results in birefringence. The required stress is obtained by introducing two identical and isolated stress applying parts (SAP), positioned in the cladding region on opposite sides of the core [27]. Therefore, no spurious mode is propagated through the SAPs,

as long as the refractive index of the SAPs is less than or equal to that of the cladding. The SAPs have different thermal expansion coefficient than that of the cladding material due to which an asymmetrical stress is applied on the fiber core after it is drawn from the preform and cooled down. The most common shapes used for the SAPs are: bow-tie shape and circular shape, which are referred to Bow-tie [28], and PANDA fibers [29] respectively as shown in Fig. 2.7. PANDA also stands for polarization maintaining and absorption reducing fiber.

### 2.3.3 PMF with Geometrical Asymmetry

These types of polarization maintaining fibers have the non-circular cross section creating axially non symmetric nature for light propagation through it. This introduces the difference of propagation constants along two orthogonal directions and hence the geometric birefringence.

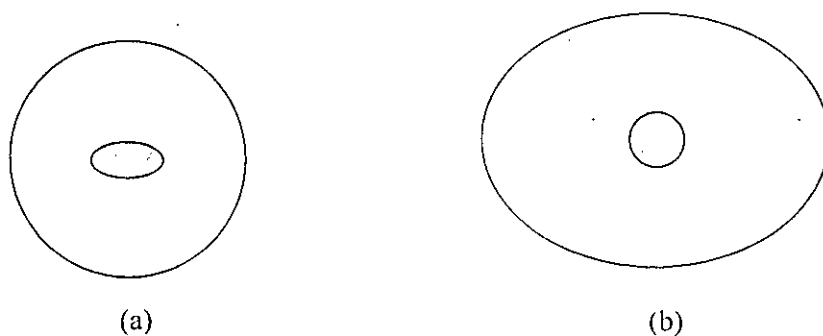


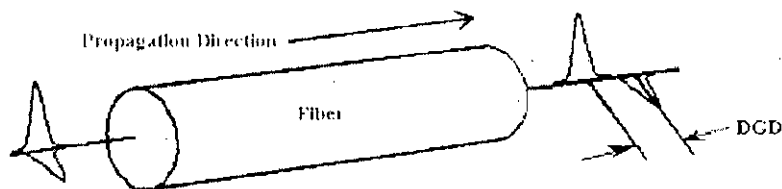
Fig. 2.8: Fiber cross section. (a) Elliptical core with circular clad. (b) Circular core with elliptical clad.

The fiber may have elliptical core with circular cladding. Elliptical cladding with circular core and elliptical jacket with circular core fiber has also been designed. The first proposal on practical low loss single polarization fiber was experimentally studied for three fiber structures: elliptical core, elliptical cladding, and elliptical jacket fibers [30]-[31]. The elliptical core and the elliptical cladding fibers were fabricated using the Modified Chemical Vapor Deposition (MCVD) method. To make elliptical clad fibers, borosilicate clad and pure silica core layers were deposited in a tube. Then the tube was collapsed while the inner pressure (vacuuming) of the tube was monitored. The core circularity and the clad ellipticity were controlled by the

careful selection of the softening points of the core/clad materials and the inner pressure. Then, the preforms were drawn into fibers. However, the elliptical jacket fiber is formed by a circular  $\text{GeO}_2\text{-P}_2\text{O}_5$  doped core and silica clad for constructing the low loss waveguide, and the  $\text{B}_2\text{O}_3$  doped elliptical jacket and the silica outer support for introducing the large nonsymmetric stress in the core.

## 2.4 Polarization Mode Dispersion and The Effect of Birefringence

In an ideal optical fiber, the core has a perfectly circular cross-section. In this case, the fundamental mode has two orthogonal polarizations (orientations of the electric field) that travel at the same speed. In a realistic fiber, however, there are random imperfections that break the circular symmetry, causing the two polarizations to propagate with different speeds and hence it is impossible to transmit data reliably at high speeds. This phenomenon is known as *Polarization Mode Dispersion (PMD)*.



So, PMD is a fundamental property of single-mode optical fiber and components that causes the broadening of the input pulse due to a phase delay between input polarization states, which increases with the increase of birefringence. In high data rate systems, PMD can significantly diminish the data-carrying capacity of a telecommunications network. It may also introduce errors as pulses spread into one another.

Conventional single-mode fibers having low birefringence have been recently found to be applicable to long-span optical transmission systems by attaching a polarization-state controller at the output end of the fiber. On the other hand, high birefringent fibers where the linear polarization state is forcedly maintained are indispensable in coherent optical transmission systems or polarization-dependent devices used in an unstable environment.

## Chapter 3

# Finite Element Method

Finite Element Analysis (FEA) was first developed in 1943 by R. Courant, who utilized the Ritz method of numerical analysis and minimization of variational calculus to obtain approximate solutions to vibration systems. Shortly thereafter, a paper published in 1956 by M. J. Turner, R. W. Clough, H. C. Martin, and L. J. Topp established a broader definition of numerical analysis. The paper centered on the "stiffness and deflection of complex structures". By the early 70's, FEA was limited to expensive mainframe computers generally owned by the aeronautics, automotive, defense, and nuclear industries. Since the rapid decline in the cost of computers and the phenomenal increase in computing power, FEA has been developed to an incredible precision. Recently, the finite element method has been exercised to a wide range of areas including electrical and electronic engineering, and many successful results have been obtained in the field of electromagnetic wave engineering as well. Among many applications of the finite element method, the research on its use with electromagnetic waveguide problems continues incessantly, and it is being established as one of the powerful numerical tools for applying electromagnetic waveguides to various waveguiding structures from microwave to optical wavelength regions.

Finite element method (FEM) is a computer based numerical technique for calculating the strength and behavior of engineering structures. It can be used to calculate deflection, stress, vibration, buckling behavior and many other phenomena. It can be used to analyze either small or large scale deflection under loading or applied displacement. It can analyze elastic deformation, or "permanently bent out of shape"

plastic deformation. The computer is required because of the astronomical number of calculations needed to analyze a large structure.

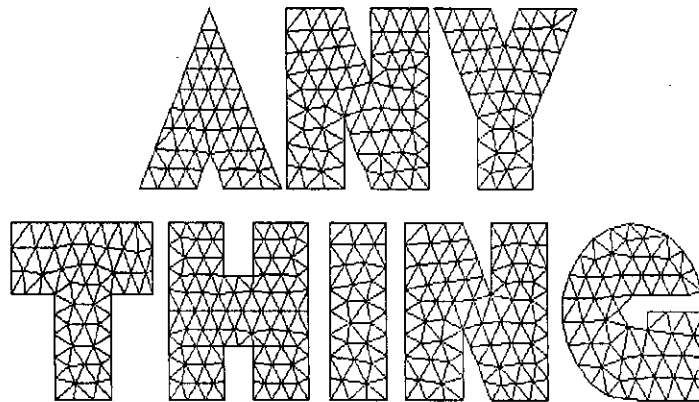


Fig. 3.1: Subdivision of structure into small element.

In the finite-element method, a distributed physical system to be analyzed is divided into a finite number (often large) of discrete elements like Fig. 3.1. The complete system may be complex and irregularly shaped, but the individual elements are easy to analyze. The division into elements may partly correspond to natural subdivisions of the structure. For example, the eardrum may be divided into groups of elements corresponding to different material properties.

From various viewpoints, electromagnetic wave problems may be classified into the following categories:

1. steady and unsteady problems
2. eigenvalue and deterministic problems
3. one, two and three dimensional problems
4. scalar and vector field problems
5. homogeneous and inhomogeneous problems
6. isotropic and anisotropic problems
7. conservative and non conservative problems
8. bounded and un bounded field problems
9. linear and non linear problems
10. forward and inverse problems

### 3.1 Boundary Value Problems

Boundary value problems arise in the mathematical modeling of physical systems and their solution has long been a major topic in mathematical physics. A typical boundary value problem can be defined by a governing differential equation in a domain  $\Omega$ :

$$L\phi = f \quad (3.1)$$

together with the boundary conditions on the boundary  $\Gamma$  that encloses the domain. In (3.1),  $L$  is a differential operator,  $f$  is the excitation or forcing function, and  $\phi$  is the unknown quantity. In electromagnetics, the Poisson's equation (3.2) is one of the examples of the differential equation (3.1).

$$-\nabla \cdot (\epsilon \nabla \phi) = \rho \quad (3.2)$$

which is the second order differential equation governing  $\phi$ , where  $\phi$  is called the scalar potential,  $\epsilon$  is the permittivity of medium,  $\rho$  is the electric charge density.

It is, of course, desirable to solve boundary value problems analytically whenever possible. However, this is generally the exception since an analytical solution can be obtained in only a few cases. In electromagnetics these include the static potential between infinite parallel plates; wave propagation in rectangular, circular, and elliptic waveguides; wave scattering by infinite planes, circular cylinders, spheres etc. Many other problems of practical importance in the engineering fields do not have an analytical solution. To overcome this difficulty, various approximate methods have been developed, and among them the Ritz and Galerkin methods have been used most widely.

### 3.2 Basic Steps of the Finite Element Method

The principle of the FEM is to replace an entire continuous domain by a number of sub-domains in which the unknown function is represented by simple interpolation

functions with unknown coefficients. Thus the original boundary value problem with an infinite number of degrees of freedom is converted into a problem with a finite number of degrees of freedom, or in other words, the solution of the whole system is approximated by a finite number of unknown coefficients. Then a set of algebraic equations or a system of equations is obtained by applying the Ritz variational or Galerkin procedure, and finally, solution of the boundary-value problem is achieved by solving the system of equations. Therefore, a finite element analysis of a boundary value problem should include the following basic steps [32]-[34]:

- (1) Discretization or subdivision of the domain
- (2) Selection of the interpolation functions
- (3) Formulation of the system of equations
- (4) Solution of the system of equations

### 3.2.1 Domain Discretization

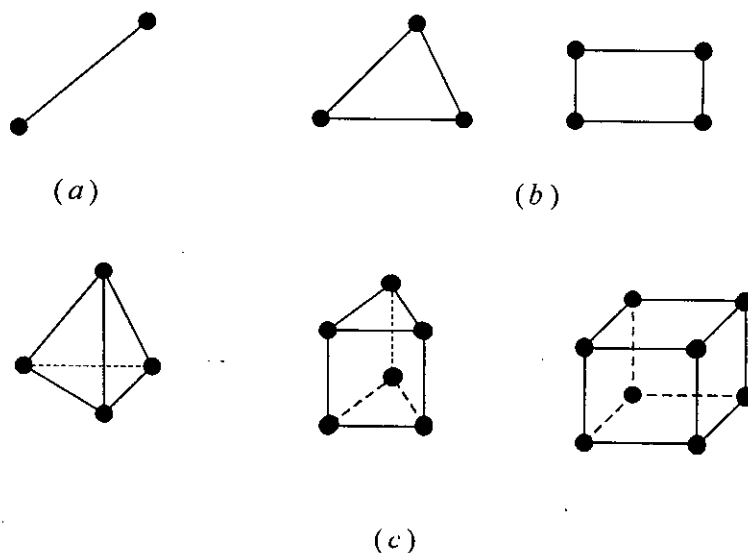


Fig. 3.2 Basic finite elements. (a) One dimensional, (b) Two dimensional, and (c) Three dimensional.

The discretization of the domain, say  $S$ , is the first and perhaps the most important step in any finite element analysis because the manner in which the domain is



discretized will affect the computer storage requirements, the computation time, and the accuracy of the numerical results [34]. In this step, the entire domain  $S$  is subdivided into a number of small domains, denoted as  $S^e$  ( $e = 1, 2, 3, \dots, M$ ), with  $M$  denoting the total number of sub-domains. These sub-domains are usually referred to as the elements. For one-dimensional domain, which is actually a straight or curve line, the elements are often short line segments interconnected to form the original line [Fig. 3.2(a)]. For a two dimensional domain, the elements are usually small triangles and rectangles [Fig. 3.2(b)]. The rectangular elements are best suited for discretizing rectangular regions, while the triangular ones can be used for irregular regions. In a three dimensional solution, the domain may be subdivided into tetrahedra, triangular prism, or rectangular bricks [Fig. 3.2(c)], among which tetrahedra are the simplest and best suited for arbitrary-volume domains. We note that the linear line segments, triangles, and tetrahedra are the basic one, two, and three-dimensional elements.

In most finite element solutions, the problem is formulated in terms of the unknown function  $\phi$  at nodes associated with the elements. For example, a linear line element has two nodes, one at each endpoint. A linear triangular element has three nodes, located at its three vertices, whereas a linear tetrahedron has four nodes, located at its four corners. For implementation it is necessary to describe these nodes. A complete description of a node contains its coordinate values, local number, and global number. The local number of the node indicates its position in the element, whereas the global number specifies its position in the entire system. The finite element formulation usually results in a banded matrix whose bandwidth is determined by the maximum difference between the global numbers of two nodes in an element. Thus, if a banded matrix solution method is employed to solve the final matrix equation, the computer storage and processing cost can be reduced significantly by properly numbering the nodes to minimize the bandwidth. However, when bandwidth minimization is unnecessary, the numbering scheme can be arbitrary and is usually chosen to simplify the programming.

In this thesis, to analyze the thermal stress of optical fiber, we decompose the one forth of fiber cross section into a number of two-dimensional triangular elements as

shown in Fig. 3.3. One fourth cross section is used for efficient use of computer memory. The basic requirement of the discretization is that there should be neither overlap nor gaps between elements. Further, elements should be connected via their vertices, or in other words, a vertex of an element can only be at the vertices of its neighboring elements; it cannot be at the side of another element. In addition to these basic requirements, a good discretization should also address the following two points. First, it should avoid the generation of narrow elements, or elements having a small inner angle. Although these elements are admissible, they can, nevertheless, increase the solution error; since, as can be shown, the error of the finite element solution is inversely proportional to the sine of the smallest inner angle. Therefore, all elements should be made close to equilateral. Second, one should note that the smaller the elements, the better the numerical solution. Since smaller elements will result in more unknowns, thus increasing the memory demand and computing time, it is necessary to keep the number of elements to the minimum for desired accuracy. A good practice is to use small elements where the solution is anticipated to have drastic variation, whereas in the regions where the variation is low the elements can be made larger.

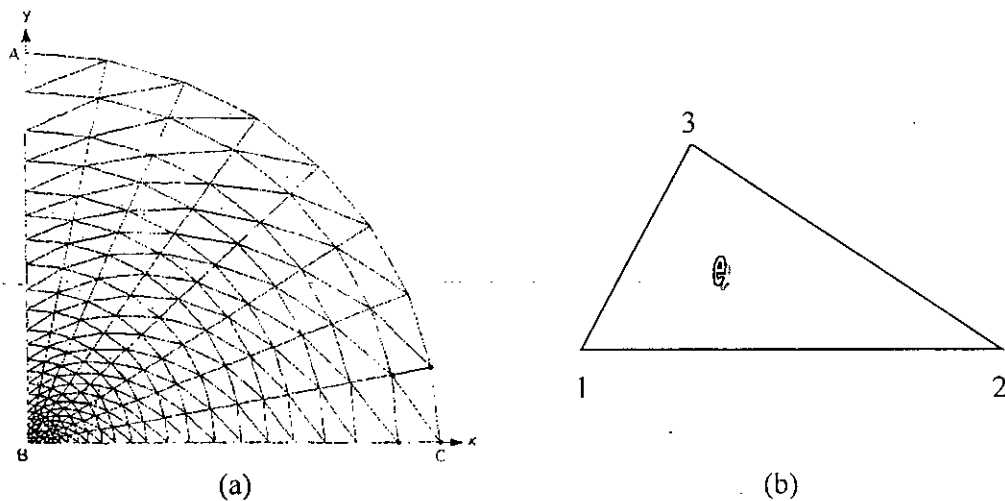
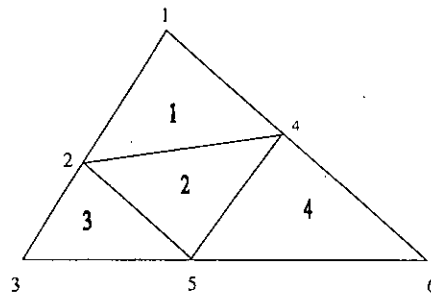


Fig. 3.3: (a) Finite element division of optical fiber. (b) Linear triangular elements.

To identify each element, we can label the elements with a set of integers, and similarly, to identify the nodes that are the vertices of the elements, we can label them with another set of integers. Since each element is related to several nodes, in this case to three nodes, a node has its own position in the associated element in addition to its position in the entire system. This position can also be labeled with an integer number, referred to as the local number, in contrast to the global number, which indicates its position in the entire system. To relate these three numbers – the global node number, the local node number, and the element number – we introduce a  $3 \times M$  integer array, denoted by  $n(i,e)$ , where  $i=1,2,3,\dots,M$ , with  $M$  denoting the total number of elements. In  $n(i,e)$ , which is also called the connectivity array,  $i$  is the local number of a node,  $e$  is the element number, and the value of  $n(i,e)$  is the global



number of the node. Obviously, this integer array includes all information concerning the numbering of the elements and nodes. To illustrate this more clearly, let us consider the example shown in Fig. 3.4. In this example we have four elements and six nodes. The array  $n(i,e)$  can be numbered as shown in table 3.1.

Fig. 3.4: Subdivision of a two dimensional domain

Table 3.1: Numbering arrangement for global number, local number and element number.

e	$n(1,e)$	$n(2,e)$	$n(3,e)$
1	2	4	1
2	5	4	2
3	3	5	2
4	5	6	4

Obviously, this numbering is not unique. For instance, we can also number the three nodes for the first elements as 4,1,2 or 1,2,4 as long as they are numbered counterclockwise so that they are consistent with the local numbering shown in Fig. 3.3(b). In addition to the connectivity array defined above, we can introduce a similar array.

### 3.2.2 Selection of Interpolation Functions

The second step of a finite element analysis is to select an interpolation function that provides an approximation of the unknown solution within an element. The interpolation is usually selected to be a polynomial of first (linear) order, second (quadratic) order, or higher order. Higher-order polynomials, although more accurate, usually result in a more complicated formulation. Hence, the simple and basic linear interpolation is still widely used. Once the order of the polynomial is selected, we can derive an expression for the unknown solution in an element, say element  $e$ , in the following form:

$$\phi^e = \sum_{j=1}^n N_j^e \phi_j^e = \{N^e\}^T \{\phi^e\} = \{\phi^e\}^T \{N^e\} \quad (3.3)$$

where  $n$  is the number of nodes in the element,  $\phi_j^e$  the value of  $\phi$  at node  $j$  of the element, and  $N_j^e$  the interpolation function, which is also known as expansion or basis function. The highest order of  $N_j^e$  is referred to as the order of the element; for example, if  $N_j^e$  is a linear function, the element  $e$  is a linear element. An important feature of the functions  $N_j^e$  is that they are nonzero only within element  $e$ , and outside this element they vanish.

As we are using linear triangular elements, the unknown function  $\phi$  within each element is approximated as

$$\phi^e(x, y) = a^e + b^e x + c^e y \quad (3.4)$$

where  $a^e$ ,  $b^e$  and  $c^e$  are constant coefficients to be determined and  $e$  is the element number. For a linear triangular element, there are three nodes located at the vertices of the triangle (Fig. 3.4). Assume that the nodes are numbered counterclockwise by numerals 1, 2 and 3, with the corresponding values of  $\phi$  denoted by  $\phi^1$ ,  $\phi^2$  and  $\phi^3$ , respectively. Enforcing (3.4) at the three nodes, we obtain

$$\phi_1^e(x, y) = a^e + b^e x_1^e + c^e y_1^e$$

$$\phi_2^e(x, y) = a^e + b^e x_2^e + c^e y_2^e$$

$$\phi_3^e(x, y) = a^e + b^e x_3^e + c^e y_3^e$$

Solving for the constant coefficients  $a^e$ ,  $b^e$  and  $c^e$  in terms of  $\phi_j^e$ , and substituting them back into (3.4) yields

$$\phi^e(x, y) = \sum_{j=1}^3 N_j^e(x, y) \phi_j^e \quad (3.5)$$

where  $N_j^e(x, y)$  are the interpolation or expansion functions given by

$$N_j^e(x, y) = \frac{1}{2\Delta^e} (a_j^e + b_j^e x + c_j^e y) \quad j = 1, 2, 3 \quad (3.6)$$

In which

$$a_1^e = x_2^e y_3^e - y_2^e x_3^e; \quad b_1^e = y_2^e - y_3^e; \quad c_1^e = x_3^e - x_2^e$$

$$a_2^e = x_3^e y_1^e - y_3^e x_1^e; \quad b_2^e = y_3^e - y_1^e; \quad c_2^e = x_1^e - x_3^e$$

$$a_3^e = x_1^e y_2^e - y_1^e x_2^e; \quad b_3^e = y_1^e - y_2^e; \quad c_3^e = x_2^e - x_1^e$$

and

$$\Delta^e = \frac{1}{2} \begin{vmatrix} 1 & x_1^e & y_1^e \\ 1 & x_2^e & y_2^e \\ 1 & x_3^e & y_3^e \end{vmatrix} = \frac{1}{2} (b_1^e c_2^e - b_2^e c_1^e)$$

= area of the eth element

In the above,  $x_j^e$  and  $y_j^e$  ( $j = 1, 2, 3$ ) denote the coordinate values of the  $j$ th node in the  $e$ th element. It can be easily shown that the interpolation functions have the property

$$N_i^e(x_j^e, y_j^e) = \delta_{ij} = \begin{cases} 1 & i = j \\ 0 & i \neq j \end{cases}$$

And, as a result at node  $i$ ,  $\phi^e$  in (3.4) reduces to its nodal value. Another important feature of  $N_j^e(x, y)$  is that it vanishes when the observation point  $(x, y)$  is on the element side opposite to the  $j$ th node. Therefore, the value of  $\phi^e$  at an element side is not related to the value of  $\phi$  at the opposite node, but rather it is determined by the values at the two endpoints of its associated side. This important feature guarantees the continuity of solution across the element sides. For better understanding Fig. 3.5 shows the interpolation functions  $N_j^e$  for a triangular element.

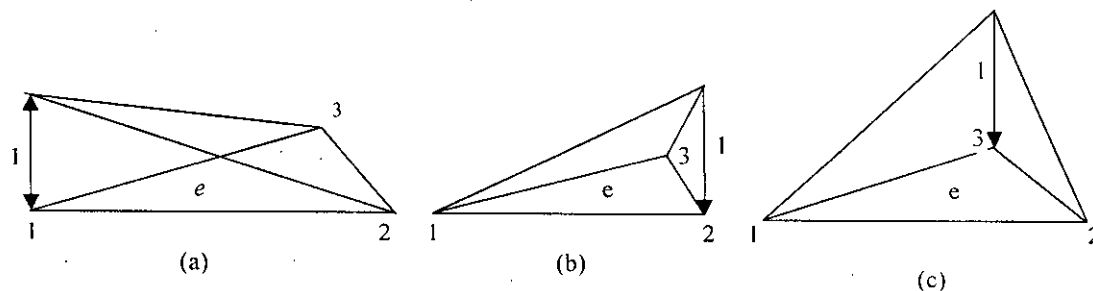


Fig 3.5: Linear interpolation functions for a triangular element. (a)  $N_1^e$ , (b)  $N_2^e$  and (c)  $N_3^e$ . The planar surfaces of the functions are shaded.

### 3.2.3 Formulation of the System of Equations

The third step, also a major step in a finite element analysis, is to formulate the system of equations. Both the Ritz variational and Galerkin methods can be used for this purpose [32]-[34].

### A. Formulation via the Ritz Method

Consider a boundary value problem defined by the differential equation

$$L\phi = f \quad (3.7)$$

If the operator  $L$  is self adjoint, i.e.,

$$\langle L\phi, \varphi \rangle = \langle \phi, L\varphi \rangle \quad (3.8)$$

and positive definite, i.e.,

$$\langle L\phi, \phi \rangle \begin{cases} > 0 & \phi \neq 0 \\ = 0 & \phi = 0 \end{cases} \quad (3.9)$$

its solution can be obtained by minimizing the functional given by

$$F(\phi) = \frac{1}{2} \langle L\phi, \phi \rangle - \frac{1}{2} \langle \phi, f \rangle - \frac{1}{2} \langle f, \phi \rangle \quad (3.10)$$

In the above,  $\varphi$  denotes an arbitrary function satisfying the same boundary conditions as does  $\phi$ . The angular bracket denotes the inner product defined by

$$\langle \phi, \varphi \rangle = \int_{\Omega} \phi \varphi^* d\Omega \quad (3.11)$$

where  $\Omega$  denotes the domain of the problem, which could be one, two or three dimensional and the asterisk denotes the complex conjugate operation.

For simplicity assume that the problem is real valued. The functional  $F$  given in (3.10) can be expressed as

$$F(\bar{\phi}) = \sum_{c=1}^M F^c(\bar{\phi}^c) \quad (3.12)$$

where  $M$  is the number of the elements comprising the entire domain and

$$F^e(\bar{\phi}^e) = \frac{1}{2} \int_{\Omega^e} \bar{\phi}^e L \bar{\phi}^e d\Omega - \int_{\Omega^e} f \bar{\phi}^e d\Omega \quad (3.13)$$

Substituting 3.3 into 3.13, we obtain

$$F^e = \frac{1}{2} \{\phi^e\}^T \int_{\Omega^e} \{N^e\} L \{N^e\}^T d\Omega \{\phi^e\} - \{\phi^e\}^T \int_{\Omega^e} f \{N^e\} d\Omega \quad (3.14)$$

which can be written in matrix form as

$$F^e = \frac{1}{2} \{\phi^e\}^T [K^e] \{\phi^e\} - \{\phi^e\}^T \{b^e\} \quad (3.15)$$

where  $[K^e]$  is an  $n \times n$  matrix and  $\{b^e\}$  an  $n \times 1$  column vector with their elements given by

$$K_{ij}^e = \int_{\Omega^e} N_i^e L N_j^e d\Omega \quad (3.16)$$

and

$$b_i^e = \int_{\Omega^e} f N_i^e d\Omega \quad (3.17)$$

We note that the elemental matrix  $[K^e]$  is symmetric since  $L$  is self-adjoint. Substituting 3.15 into 3.12, we obtain

$$F(\bar{\phi}) = \sum_{e=1}^M \left( \frac{1}{2} \{\phi^e\}^T [K^e] \{\phi^e\} - \{\phi^e\}^T \{b^e\} \right) \quad (3.18)$$

and by performing the summation and adopting the global node numbers, this can be written as

$$F = \frac{1}{2} \{\phi\}^T [K] \{\phi\} - \{\phi\}^T \{b\} \quad (3.19)$$

where  $[K]$  is an  $N \times N$  symmetric matrix with  $N$  being the total number of unknowns or nodes,  $\{\phi\}$  an  $N \times 1$  unknown vector whose elements are the unknown expansion coefficients, and  $\{b\}$  an  $N \times 1$  known vector. The system of equations is



then obtained by imposing the stationarity requirement  $\delta F = 0$ , or equivalently, by setting the partial derivative of  $F$  with respect to  $\phi$  to zero:

$$\frac{\partial F}{\partial \phi_i} = \frac{1}{2} \sum_{j=1}^N (K_{ij} + K_{ji}) \phi_j - b_i = 0 \quad i = 1, 2, 3, \dots, N. \quad (3.20)$$

Since  $[K]$  is symmetric,  $K_{ij} = K_{ji}$  and therefore (2.20) becomes

$$\frac{\partial F}{\partial \phi_i} = \sum_{j=1}^N K_{ij} \phi_j - b_i = 0 \quad i = 1, 2, 3, \dots, N. \quad (3.21)$$

or the matrix form will be given by

$$[K]\{\phi\} = \{b\} \quad (3.22)$$

### ***B. Formulation via Galerkin's Method***

The system of equations above can also be formulated via Galerkin's method. According to this method, the residual  $R$  for each node in an element is [35]

$$R_i^e = \int_{\Omega_e} N_i^e (L\bar{\phi}^e - f) d\Omega \quad i = 1, 2, 3, \dots, n. \quad (3.23)$$

Substituting (3.3) into (3.23), then yields

$$R_i^e = \int_{\Omega_e} N_i^e L \{N^e\}^T d\Omega \{\phi\} - \int_{\Omega_e} f N_i^e d\Omega \quad i = 1, 2, 3, \dots, n. \quad (3.24)$$

which can again be written in matrix form as

$$\{R^e\} = [K^e] \{\phi^e\} - \{b^e\} \quad (3.25)$$

We may expand (3.25) using the local and global relations and then sum it over each element to find that

$$\{R\} = \sum_{e=1}^M \{R^e\} = \sum_{e=1}^M \left( [K^e] \{\phi^e\} - \{b^e\} \right) \quad (3.26)$$

The system of equations can then be obtained by setting (3.26) to zero, resulting in

$$\sum_{e=1}^M \left( [K^e] \{\phi^e\} - \{b^e\} \right) = \{0\} \quad (3.27)$$

which can again be written in the form of (3.22) i.e.

$$[K] \{\phi\} = \{b\} \quad (3.28)$$

Before the system of equations (3.28) is ready to be solved for a specific solution, we need to apply the required boundary conditions. There are two kinds of boundary conditions that are often encountered: one is the Dirichlet boundary condition, which prescribes  $\phi$  at the boundary, and the other is the homogeneous Neumann boundary condition, which requires the normal derivative of  $\phi$  to vanish at the boundary. The first is an essential boundary condition that must be imposed explicitly, in contrast to the second, which is usually satisfied implicitly and automatically in the solution process. For this reason, the second one is often called the natural boundary condition.

It is seen that in this step we actually have three sub-steps. First, we formulate the elemental equation (3.15) or (3.25) using either of the two methods. Then, we sum the elemental equations over all elements to form the system of equations and this process is called assembly. Finally, we impose the boundary conditions to obtain the final form of the system of equations. We note that in computer implementation, the three sub-steps are usually not separated; in stead, they are intertwined. The generation of the elemental matrix and the imposition of the boundary conditions usually take place during the process of assembly.

### 3.2.4 Solution of the System of Equations

Solving the system of equations is the final step in a finite element analysis. The resultant system has one of the following two forms:

$$[K]\{\phi\} = \{b\} \quad (3.29)$$

or

$$[A]\{\phi\} = \lambda[B]\{\phi\} \quad (3.30)$$

Equation (3.29) is of the deterministic type, resulting from either an inhomogeneous differential equation or inhomogeneous boundary conditions or both.

In electromagnetics, deterministic systems are usually associated with scattering, radiation, and other deterministic problems where there exists a source or excitation. To the contrary, (3.30) is of the eigenvalue type, resulting from a homogeneous governing differential equation and homogeneous boundary conditions. In electromagnetics, eigenvalue systems are usually associated with source free problems such as wave propagation in waveguides and resonance in cavities. In this case, the known vector  $\{b\}$  vanishes and the matrix  $[K]$  can be written as  $[A] - \lambda[B]$ , where  $\lambda$  denotes the unknown eigenvalues. Once we have solved the system of equations for  $\{\phi\}$ , we can then compute the desired parameters, such as capacitance, inductance, input impedance, and scattering or radiation patterns and display the result in form of curves, plots, or color pictures, which are more meaningful interpretable. This final stage, often referred to as post-processing, can also be separated completely from the other steps.

## Chapter 4

# Stress Analysis of Optical Fiber

### 4.1 Introduction

Generally speaking, optical fibers are produced in an atmosphere at very high temperature. Therefore, when the fibers are cooled down to room temperature, stresses are developed if the materials used have different thermal expansion coefficients. In the fabrication of non-symmetrical fiber, such as bow-tie fiber, PANDA fiber, side-hole fiber, *etc.*, the change of temperature during the cooling stage produces stress, which in turn introduces a non-symmetrical refractive index change due to the elasto-optic effect. Also, external forces can be applied to produce deliberate stresses in the fiber itself. Furthermore, in underwater communication systems, the fiber undergoes very large hydraulic pressure. So, the stress analysis of fiber is important in order to take the photo-elastic effect into account and it requires the understanding of energy principle.

### 4.2 Energy principle

The energy principle states that the total potential energy should be a minimum when thermal stress and/or an external force is applied to the body. In other words, the strain distribution that is actually generated among all possible strain profiles is the distribution that makes the potential energy a minimum. The total potential energy of the body is given by [8], [15]

$$\Pi = (\text{internal work}) - (\text{external work}) = U - V, \quad (4.1)$$

where  $U$  and  $V$  denote strain energy and work done by the external force, respectively. Strain energy  $U$  is work generated during the process of releasing strain; *i.e.*,  $U$  is a summation of {local force generated under certain strain condition}  $\times$  {displacement by the force}. Since potential energy decreases by the amount of work done by the external force,  $V$  has a minus sign in (4.1).

Stress analysis based on the energy principle is called the energy method. The finite element method (FEM) based calculation procedure is as follows:

- Express the potential energy  $\Pi$  in terms of the displacement by strain and an external force.
- Approximate the displacement and external force in or toward each element by analytical functions using values at nodal points.
- Apply the energy principle to  $\Pi$ ; *i.e.*, partially differentiate  $\Pi$  with respect to the displacement and obtain an equilibrium equation (linear simultaneous equations).
- Solve the simultaneous equations and determine the displacement at each nodal point.
- The strain and stress in each element are calculated by using the displacement at the nodes surrounding the element.

### 4.3 Stresses and strain in optical fibers

The optical fiber is always very long in one dimension (along  $z$ -axis direction) and very limited in the other two transverse dimensions. In such a case, strain in the body along  $z$ -axis  $\varepsilon_z$  is considered to be negligible, except at both ends. Thus, we can assume

$$\varepsilon_z = 0. \quad (4.2)$$

Stress analysis based on this assumption is called a "plane strain problem" [8],[15]. The relationship between displacement and strain is given by

$$\varepsilon_x = \frac{\partial u}{\partial x}, \quad (4.3a)$$

$$\varepsilon_y = \frac{\partial v}{\partial y}, \quad (4.3b)$$

$$\text{and } \gamma_{xy} = \frac{\partial v}{\partial x} + \frac{\partial u}{\partial y}. \quad (4.3c)$$

Here  $u$  and  $v$  are displacements along the  $x$ - and  $y$ -axis directions, respectively, and are in general approximated as functions of  $x$  and  $y$ .  $\varepsilon_x$ ,  $\varepsilon_y$ , and  $\varepsilon_z$  are spatial variations of the principal strains along the  $x$ -,  $y$ -, and  $z$ -axis directions, respectively, and  $\gamma_{xy}$  is the shear strain in the  $x$ - $y$  plane. For linear elastic material, the stress-strain relations come from generalized Hooke's law. For isotropic materials, the two material properties are the Young's modulus (or modulus of elasticity) and the Poisson's ratio. Another type of deformation occurs in the body which is due to the temperature change. For isotropic material change in temperature results in a uniform strain, which depends on the coefficient of linear expansion  $\alpha$  of the material.  $\alpha$ , which represents the change in length per unit temperature change, is always assumed to be constant within the range of variation of the temperature. Also, this strain does not cause any stresses when the body is free of deform. The temperature strain is usually considered as an initial strain. Therefore, combining the Hooke's law and the temperature strain, the relationship between the stress and the strain is generally expressed as [8], [15].

$$\varepsilon_x = \frac{1}{E}[\sigma_x - \mu(\sigma_y + \sigma_z)] + \alpha \Delta T, \quad (4.4a)$$

$$\varepsilon_y = \frac{1}{E}[\sigma_y - \mu(\sigma_z + \sigma_x)] + \alpha \Delta T, \quad (4.4b)$$

$$\varepsilon_z = \frac{1}{E}[\sigma_z - \mu(\sigma_x + \sigma_y)] + \alpha \Delta T, \quad (4.4c)$$

$$\gamma_{xy} = \frac{\tau_{xy}}{G} = \frac{2(1+\mu)}{E} \tau_{xy}, \quad (4.5)$$

where  $\sigma_x$ ,  $\sigma_y$ , and  $\sigma_z$  are spatial variations of the principal stresses along the  $x$ -,  $y$ -, and  $z$ -axis directions, respectively,  $\tau_{xy}$  is the shear stress in the  $x$ - $y$  plane,  $G$ ,  $\alpha$ , and  $\Delta T$  denote the shear modulus (or modulus of rigidity), the thermal expansion coefficient, and the temperature change (negative for cooling), respectively,  $E$  and  $\mu$  are the Young's modulus and the Poisson's ratio, respectively. Considering the problem to be a 'plane strain problem', we can get the following relations between the stress and the strain

$$\sigma_x = \frac{E}{(1+\mu)(1-2\mu)} \left[ (1-\mu)\varepsilon_x + \mu\varepsilon_y \right] - \frac{\alpha E \Delta T}{(1-2\mu)}, \quad (4.6a)$$

$$\sigma_y = \frac{E}{(1+\mu)(1-2\mu)} \left[ \mu\varepsilon_x + (1-\mu)\varepsilon_y \right] - \frac{\alpha E \Delta T}{(1-2\mu)}, \quad (4.6b)$$

$$\sigma_z = \mu(\sigma_x + \sigma_y) - \alpha E \Delta T. \quad (4.6c)$$

For “plane strain problem”, the components of stress and strain are expressed in vector form as

$$\{\sigma\} = \begin{bmatrix} \sigma_x \\ \sigma_y \\ \tau_{xy} \end{bmatrix}, \quad (4.7)$$

$$\{\varepsilon\} = \begin{bmatrix} \varepsilon_x \\ \varepsilon_y \\ \gamma_{xy} \end{bmatrix}. \quad (4.8)$$

Using (4.7)-(4.8), the relationship between the stress and the strain of the “plane strain problem” as defined by (4.5) and (4.6), can be expressed as

$$\{\sigma\} = [D](\{\varepsilon\} - \{\varepsilon_0\}), \quad (4.9)$$

where the  $3 \times 1$  initial strain vector  $\{\varepsilon_0\}$  due to the thermal strain and the  $3 \times 3$  matrix  $[D]$  are given by

$$\{\varepsilon_0\} = (1+\mu)\alpha \Delta T \begin{bmatrix} 1 \\ 1 \\ 0 \end{bmatrix}, \quad (4.10)$$

and

$$[D] = \frac{E}{(1+\mu)(1-2\mu)} \begin{bmatrix} (1-\mu) & \mu & 0 \\ \mu & (1-\mu) & 0 \\ 0 & 0 & (1-2\mu)/2 \end{bmatrix}. \quad (4.11)$$

#### 4.4 Mathematical Formulation

Strain energy per unit length is obtained by

$$(\text{strain energy}) = \frac{1}{2} \iint (\text{stress}) \cdot [(\text{strain}) - (\text{initial strain})] dx dy.$$

Then, 
$$U = \frac{1}{2} \iint \{\sigma\}^T [\{\varepsilon\} - \{\varepsilon_0\}] dx dy, \quad (4.12)$$

where  $\{\cdot\}^T$  represents the transpose of the vector and integration is over the cross-section of the actual structural body under strain and stress. Since strain and stress do not penetrate into the air region, the actual boundary of the body becomes the boundary of the FEM analysis. The displacements  $u(x, y)$  and  $v(x, y)$  along the  $x$ - and  $y$ -axis directions in the  $e$ th ( $e = 1-N$ ) element is approximated by the linear function of  $x$  and  $y$ :

$$u(x, y) = p_0^e + p_1^e x + p_2^e y, \quad (4.13a)$$

$$v(x, y) = q_0^e + q_1^e x + q_2^e y, \quad (4.13b)$$

where  $p_0^e, p_1^e, p_2^e$  and  $q_0^e, q_1^e, q_2^e$  are expansion coefficients. Assuming the displacements at nodal points  $i, j$ , and  $k$  in the  $e$ th element are given by  $(u_i, v_i), (u_j, v_j)$  and  $(u_k, v_k)$ , respectively, the expansion coefficients  $p$ 's and  $q$ 's are obtained by solving the linear equations which can be obtained from (4.13) for the nodal displacements corresponding to the 3 nodal points  $i, j$ , and  $k$  of the  $e$ th element. Thus, one can obtain

$$\begin{bmatrix} p_0^e \\ p_1^e \\ p_2^e \end{bmatrix} = [C^e] \begin{bmatrix} u_i \\ u_j \\ u_k \end{bmatrix}, \quad (4.14a)$$

$$\begin{bmatrix} q_0^e \\ q_1^e \\ q_2^e \end{bmatrix} = [C^e] \begin{bmatrix} v_i \\ v_j \\ v_k \end{bmatrix}, \quad (4.14b)$$

where  $[C^e]$  is given by

$$[C^e] = \begin{bmatrix} 1 & x_i & y_i \\ 1 & x_j & y_j \\ 1 & x_k & y_k \end{bmatrix}^{-1},$$

$$i.e., \quad [C^e] = \frac{1}{2s_e} \begin{bmatrix} (x_j y_k - x_k y_j) & (x_k y_i - x_i y_k) & (x_i y_j - x_j y_i) \\ (y_j - y_k) & (y_k - y_i) & (y_i - y_j) \\ (x_k - x_j) & (x_i - x_k) & (x_j - x_i) \end{bmatrix}. \quad (4.15)$$

Here, the coordinates of the nodal points of the triangular element are expressed as  $(x_m, y_m)$  ( $m = i, j, k$ ). Hence, the cross-sectional area  $s_e$  of the  $e$ th element is given by

$$2s_e = (x_j - x_i)(y_k - y_i) - (x_k - x_i)(y_j - y_i).$$



Now, we find the strain components in the  $e$ th element as

$$\begin{aligned}\varepsilon_x &= \frac{\partial u}{\partial x} = p_1^e = \frac{1}{2s_e} [(y_j - y_k)u_i + (y_k - y_i)u_j + (y_i - y_j)u_k], \\ \varepsilon_y &= \frac{\partial v}{\partial y} = q_2^e = \frac{1}{2s_e} [(x_k - x_j)v_i + (x_i - x_k)v_j + (x_j - x_i)v_k], \\ \gamma_{xy} &= \frac{\partial v}{\partial x} + \frac{\partial u}{\partial y} = q_1^e + p_2^e = \frac{1}{2s_e} [(y_j - y_k)v_i + (y_k - y_i)v_j + (y_i - y_j)v_k] + \\ &\quad \frac{1}{2s_e} [(x_k - x_i)u_i + (x_i - x_k)u_j + (x_j - x_i)u_k].\end{aligned}$$

Therefore, we get the strain vector in each element as

$$\begin{bmatrix} \varepsilon_x \\ \varepsilon_y \\ \gamma_{xy} \end{bmatrix} = \frac{1}{2s_e} \begin{bmatrix} (y_j - y_k) & 0 & (y_k - y_i) & 0 & (y_i - y_j) & 0 \\ 0 & (x_k - x_j) & 0 & (x_i - x_k) & 0 & (x_j - x_i) \\ (x_k - x_j) & (y_j - y_k) & (x_i - x_k) & (y_k - y_i) & (x_j - x_i) & (y_i - y_j) \end{bmatrix} \begin{bmatrix} u_i \\ v_i \\ u_j \\ v_j \\ u_k \\ v_k \end{bmatrix}. \quad (4.16)$$

This is rewritten in matrix form as

$$\{\varepsilon^e\} = [B^e] \{d^e\}, \quad (4.17)$$

where  $[B^e]$  is a  $3 \times 6$ -element matrix in the right-hand side of (4.16) and  $\{d^e\}$  represents the displacement vector, a  $6 \times 1$  column matrix having six degrees of freedom for  $e$ th element, *i.e.*,

$$[B^e] = \frac{1}{2s_e} \begin{bmatrix} (y_j - y_k) & 0 & (y_k - y_i) & 0 & (y_i - y_j) & 0 \\ 0 & (x_k - x_j) & 0 & (x_i - x_k) & 0 & (x_j - x_i) \\ (x_k - x_j) & (y_j - y_k) & (x_i - x_k) & (y_k - y_i) & (x_j - x_i) & (y_i - y_j) \end{bmatrix},$$

and

$$\{d^e\} = \begin{bmatrix} u_i \\ v_i \\ u_j \\ v_j \\ u_k \\ v_k \end{bmatrix}.$$

The strain energy in the  $e$ th element is then expressed as

$$U^e = \frac{1}{2} \iint \{\sigma^e\}^T [\{\varepsilon^e\} - \{\varepsilon_0^e\}] dx dy. \quad (4.18)$$

From (3.9),  $\{\sigma^e\}^T$  of (3.18) can be expressed as

$$\{\sigma^e\}^T = [\{\varepsilon^e\}^T - \{\varepsilon_0^e\}^T] [D^e]^T = [\{d^e\}^T [B^e]^T - \{\varepsilon_0^e\}^T] [D^e]^T. \quad (4.19)$$

Here,  $[D^e] \equiv [D^e]^T$  and the element matrix  $[D^e]$  may be different in each element, since the Young's modulus and the Poisson's ratio are different in different materials (the core and substrate regions). Also, note that if  $[A] = [B][C]$ , then  $[A]^T = [C]^T [B]^T$ . Now, using (4.18), (4.19) can be expressed as

$$\begin{aligned} U^e &= \frac{1}{2} \iint_c \left( \{d^e\}^T [B^e]^T [D^e]^T [B^e] \{d^e\} - \right. \\ &\quad \left. 2\{d^e\}^T [B^e]^T [D^e]^T \{\varepsilon_0^e\} + \{\varepsilon_0^e\}^T [D^e]^T \{\varepsilon_0^e\} \right) dx dy \\ &= \frac{s_e}{2} \left( \{d^e\}^T [B^e]^T [D^e]^T [B^e] \{d^e\} - 2\{d^e\}^T [B^e]^T [D^e]^T \{\varepsilon_0^e\} + \{\varepsilon_0^e\}^T [D^e]^T \{\varepsilon_0^e\} \right). \end{aligned}$$

For the last term of the above equation, we can find that

$$\{\varepsilon_0^e\}^T [D^e]^T \{\varepsilon_0^e\} = \frac{2(1+\mu_e)E_e}{(1-2\mu_e)} (\alpha_e \Delta T)^2. \quad (4.20)$$

Here  $E_e$ ,  $\mu_e$ , and  $\alpha_e$  are the Young's modulus, the Poisson's ratio, and the thermal expansion coefficient of the element. Since (4.20) is always positive, it can be neglected in the minimization process of potential energy. Then the strain energy  $U^e$  in the  $e$ th element is expressed as

$$U^e = \frac{1}{2} \{d^e\}^T [A^e] \{d^e\} - \{d^e\}^T \{h^e\}. \quad (4.21)$$

Here  $[A^e]$  is a  $6 \times 6$ -element stiffness matrix and  $\{h^e\}$  is a  $6 \times 1$  thermal stress vector, which are given by

$$[A^e] = s_e [B^e]^T [D^e]^T [B^e], \quad (4.22)$$

and 
$$\{h^e\} = s_e [B^e]^T [D^e]^T \{\varepsilon_0^e\}. \quad (4.23)$$

The total strain energy is then obtained by summing the element strain energy:

$$U = \sum_{e=1}^N U^e = \frac{1}{2} \{d\}^T [A] \{d\} - \{d\}^T \{H\}, \quad (4.24)$$

where  $\{d\}$ ,  $[A]$ , and  $\{H\}$  are the  $2n \times 1$  global strain vector, the  $2n \times 2n$  global stiffness matrix, and the  $2n \times 1$  global thermal stress vector, respectively.

An external force applied to the body is approximated by the force concentrated at the node on the surface of the body. Then the vector of the external force is expressed by

$$\{f_L'\} = \begin{bmatrix} f_1 \\ g_1 \\ f_2 \\ g_2 \\ \vdots \\ f_n \\ g_n \end{bmatrix}, \quad (4.25)$$

where  $n$  is the number of nodes on the surface of the body,  $f_i$  and  $g_i$  denote the  $x$ - and  $y$ -axis components of the external force applied to nodal point  $i$ . When a displacement  $(u_i, v_i)$  is generated by the external force  $(f_i, g_i)$ , the work done by the force is  $(u_i f_i + v_i g_i)$ . The total work done by the external force is then given by

$$V' = \{d'\}^T \{f_L'\}.$$

Here  $\{d'\}$  is the displacement vector comprised of  $u_i$ 's and  $v_i$ 's of  $n$  nodes on the surface under stress. However, in order to add up the energy of the external force to the total potential energy, we have to find the work done from all the nodal contributions such that

$$V = \{d\}^T \{f_L\}, \quad (4.26)$$

where in finding  $V$ , the force on nodes other than the nodes on surface must be zero, so that  $V=V'$ . Therefore,  $\{f_L\}$  is the global load vector acting on each nodal point.

Now, the total potential energy is given by

$$\Pi = U - V = \frac{1}{2} \{d\}^T [A] \{d\} - \{d\}^T [\{H\} + \{f_L\}]. \quad (4.27)$$

For the thermal stress analysis of birefringent fibers and wave guides without external force, we simply make  $\{f_L\} = \{0\}$ .

Potential energy should be a minimum by the energy principle. Therefore, the partial derivative of  $\Pi$  with respect to the displacement of each nodal point should be zero:

$$\text{i.e.,} \quad \frac{\partial \Pi}{\partial \{d\}} = [A] \{d\} - \{H\} - \{f_L\} = 0.$$

We then have the  $2n$ th-order linear simultaneous equations:

$$[A] \{d\} = \{H\} + \{f_L\}. \quad (4.28)$$

For the global system, now it can be written that

$$\begin{aligned} [A] &= \sum_{e=1}^N \iint [B^e]^T [D^e] [B^e] dx dy, \\ \{H\} &= \sum_{e=1}^N \iint [B^e]^T [D^e] \{\varepsilon_0^e\} dx dy. \end{aligned}$$

The solution of (4.28) gives the displacements at all nodal points of the fiber or waveguide under thermal stress and/or external forces. The solution of the displacement vector can be easily obtained as:

$$\{d\} = [A]^{-1} [\{H\} + \{f_L\}]. \quad (4.29)$$

General sparse matrix solver may be employed to solve the system of linear simultaneous equations in order to find the displacement vector. Once the displacement of each node is known, the stress in each element is calculated by

$$\{\sigma^e\} = [D^e] \left( [B^e] \{d^e\} - \{\varepsilon_0^e\} \right). \quad (e = 1-N) \quad (4.30)$$

However, in solving the linear simultaneous equations, the boundary conditions should be taken into account very carefully. Also, symmetry conditions can be used to reduce memory and time of computation in the case of finite element analysis.

In optical fibers or waveguides under stress or strain, the original refractive index of the material changes due to the photoelastic effect. The new refractive index for  $x$ - and  $y$ -polarized light can be calculated from the following equation [7]-[8], [15]:

$$\begin{bmatrix} n_x(x, y) \\ n_y(x, y) \\ n_z(x, y) \end{bmatrix} = \begin{bmatrix} n_{x0}(x, y) \\ n_{y0}(x, y) \\ n_{z0}(x, y) \end{bmatrix} - \begin{bmatrix} C_1 & C_2 & C_2 \\ C_2 & C_1 & C_2 \\ C_2 & C_2 & C_1 \end{bmatrix} \begin{bmatrix} \sigma_x(x, y) \\ \sigma_y(x, y) \\ \sigma_z(x, y) \end{bmatrix}. \quad (4.31)$$

Here  $C_1$ ,  $C_2$  are the elasto-optic (photoelastic) coefficients of the fiber or waveguide material.  $n_{x0}$ ,  $n_{y0}$ , and  $n_{z0}$  are the unstressed refractive indices of the material and  $n_x$ ,  $n_y$ , and  $n_z$  are the main diagonal elements of the anisotropic refractive index tensor. Since the material considered here is silica, an isotropic material for the fiber, having a refractive index,  $n$ , we have in this case

$$n_{x0}(x, y) = n_{y0}(x, y) = n_{z0}(x, y) = n \quad (4.32)$$

Once the stress analysis is performed, the anisotropic refractive index components can be calculated. Thus, the refractive index distribution over the cross-section of the fiber under stress is known. Therefore, the vector finite element method can then be employed to find the modal solutions of quasi-TE ( $H_{11}^y$ ) and quasi-TM ( $H_{11}^x$ ) modes. The details of the vector FEM can be found in the literature.

However, after the stress analysis, the birefringence can be calculated from the refractive indices for the  $x$ - and  $y$ -polarizations. Because the stress is distributed across the whole cross section of the fiber or waveguide, the birefringence is evaluated from the average tensor refractive indices in the core region and also the values at the center of the core [7].

Thus,

$$\bar{n}_x = \frac{1}{A} \iint_A n_x(x, y) dx dy.$$

$$\bar{n}_y = \frac{1}{A} \iint_A n_y(x, y) dx dy.$$

where  $A$  is the area of the core region. Therefore,

$$B_{average} = \bar{n}_x - \bar{n}_y = \frac{C_2 - C_1}{A} \iint_A (\sigma_y - \sigma_x) dx dy. \quad (4.33)$$

Sometimes, the birefringence of the fiber is approximated by the difference of refractive indices at the center of the fiber core [7]. Assuming that the center of the core is the origin of the coordinate system, we can write

$$B_0 = n_x(0, 0) - n_y(0, 0) = (C_2 - C_1)(\sigma_y - \sigma_x) \Big|_{x=0, y=0}. \quad (4.34)$$

## Chapter 5

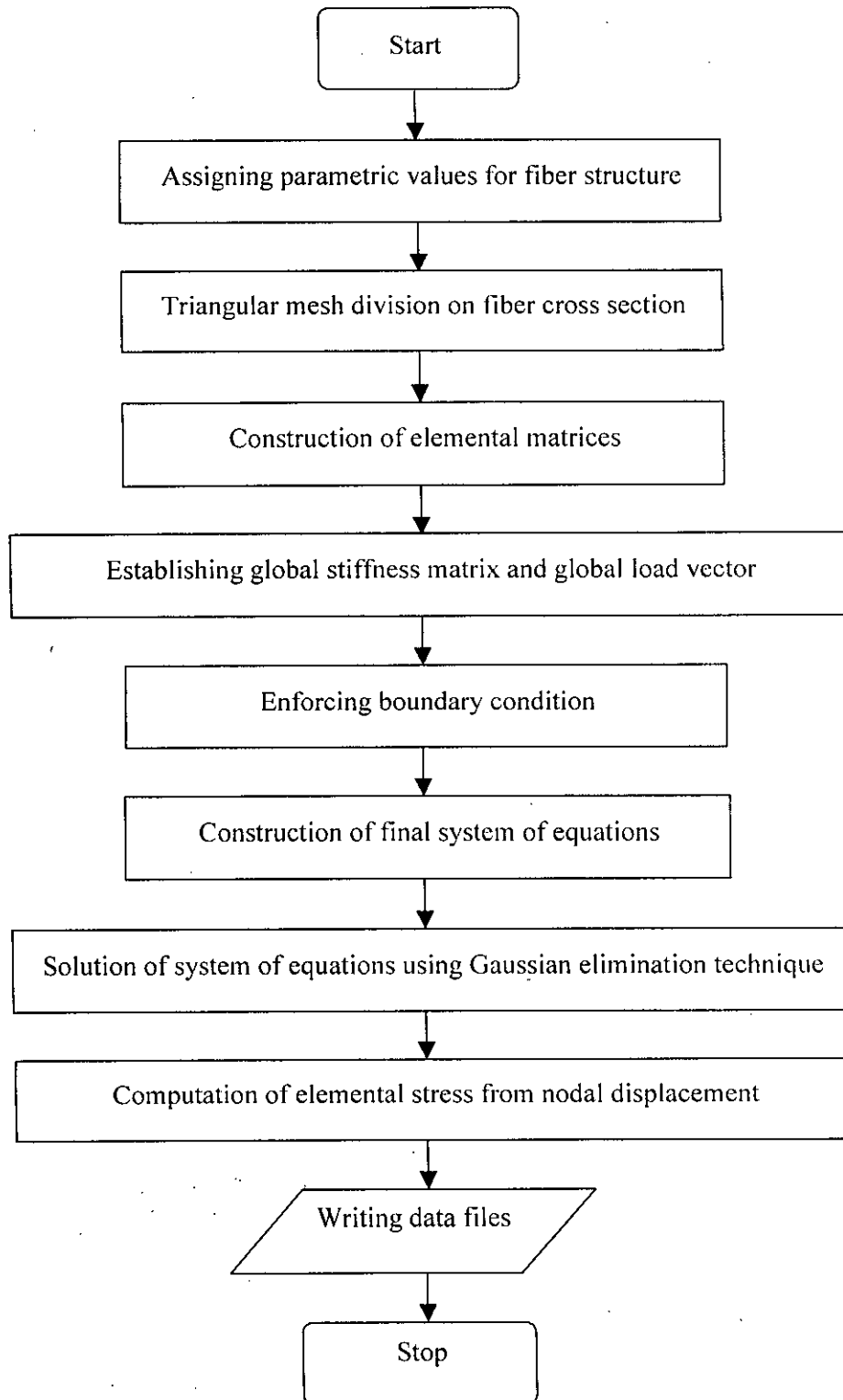
# Numerical Results and Discussions

### 5.1 Structure of the System

A simulation program based on the FEM of previous chapter has been developed for the thermal stress analysis of different optical fibers. The birefringence properties, stress and refractive index distributions were investigated thoroughly in this work. Though the target was the side-hole fiber, at first we carried out the thermal analysis on a single fiber structure and verified our calculated results by comparing with the exact analytical results. The program was written in FORTRAN77 on a windows based PC platform. Before showing the numerical results, a brief discussion on the basic structure of the system that we have developed here, has been presented in the form of a flow diagram below.

We started our analysis by setting values for fiber parameters that define the cross section of the structure and the type of fiber material. The next but very important step is to divide the cross section of the fiber into small elements of finite numbers. As the accuracy of the solution using FEM depends on the number of elements and the density of elements on or near the discontinuity of the material, only one fourth of the cross section is discretized. Then the matrices of the simultaneous linear system of equations are constructed from the elemental matrices. At this stage, the appropriate boundary conditions for nodal displacement on the plane of symmetries are applied. The final system is then solved numerically using Gaussian elimination technique. Once the nodal displacement is known, it is straightforward to calculate the stress developed in each element and also the *Birefringence* in terms of  $x$  and  $y$  polarized

light. We wrote these data into data files and MATLAB, ORIGIN are used for further processing and plotting the results.





## 5.2 Results and Discussions

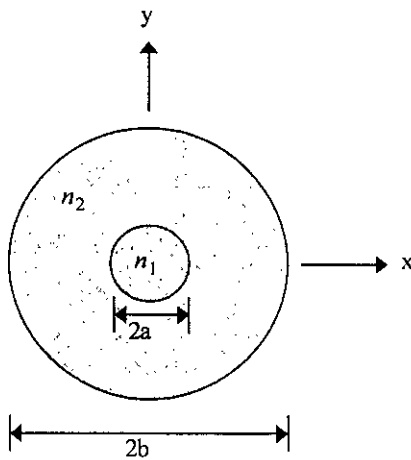
Before conducting the stress analysis of noncircular core fibers, circular fibers under thermal stress are analyzed. Since the stress distributions of fibers under thermal stress are analytically obtainable, it can be used to test the accuracy and effectiveness of the developed program. For a circular fiber under thermal stress, the stress distributions are given as follow [8],[15]:

$$\sigma_r = \begin{cases} \frac{(b^2 - a^2) (\alpha_2 - \alpha_1)}{2b^2 (1-\nu)} E \Delta T & (0 \leq r \leq a) \\ \frac{a^2 (\alpha_2 - \alpha_1)}{2b^2 (1-\nu)} E \Delta T \left( \frac{b^2}{r^2} - 1 \right) & (a \leq r \leq b) \end{cases}$$

$$\sigma_\theta = \begin{cases} \frac{(b^2 - a^2) (\alpha_2 - \alpha_1)}{2b^2 (1-\nu)} E \Delta T & (0 \leq r \leq a) \\ - \frac{a^2 (\alpha_2 - \alpha_1)}{2b^2 (1-\nu)} E \Delta T \left( \frac{b^2}{r^2} + 1 \right) & (a \leq r \leq b) \end{cases}$$

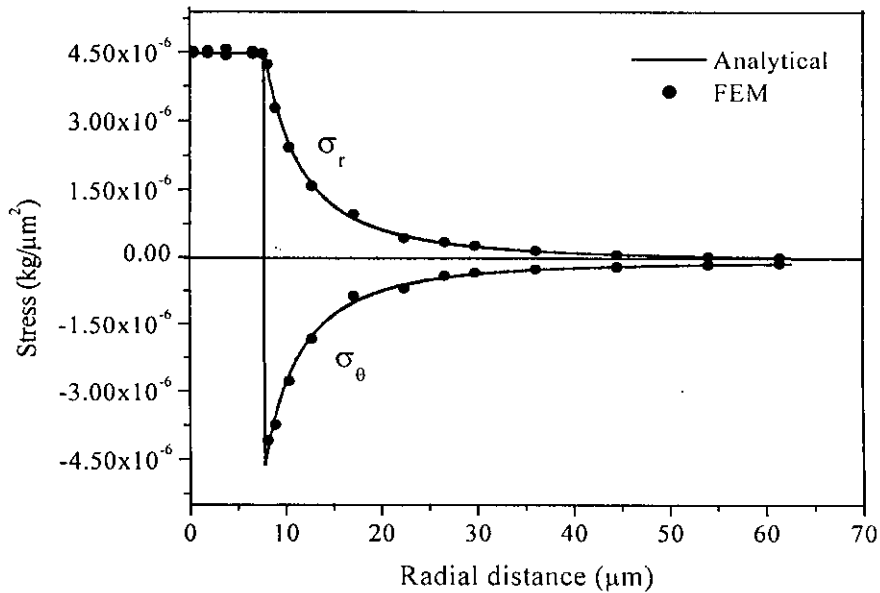
where  $a$  and  $b$  denote the core and cladding radii of the fiber.  $E$ ,  $\nu$  (nu) and  $\Delta T$  are Young's modulus, Poisson's ratio and the temperature change.  $\alpha_1$  and  $\alpha_2$  are the thermal expansion coefficient for core and cladding materials.  $n_1$  and  $n_2$  are refractive indices of core and cladding and  $C_1$ ,  $C_2$  are elasto-optic coefficient respectively.

First, let us consider a fiber with a circular core as shown in Fig. 5.1(a). The cross sectional dimensions and the material parameters are shown just beside the structure in the figure. For this simple structure, the  $\sigma_r$  and  $\sigma_\theta$  are calculated analytically using the above equations and the numerical results are obtained using the method described in the previous chapter. Our numerical results agreed well with the analytical result and the program was verified.



$a$	$= 7.8 \mu\text{m}$
$b$	$= 62.5 \mu\text{m}$
$E$	$= 0.007830 \text{ Kg}/\mu\text{m}^2$
$\nu$	$= 0.186$
$\alpha_1$	$= 14.85 \times 10^{-7} / ^\circ\text{C}$
$\alpha_2$	$= 5.4 \times 10^{-7} / ^\circ\text{C}$
$\Delta T$	$= -1000.0 ^\circ\text{C}$
$n_1$	$= 1.45$
$n_2$	$= 1.4433$
$C_1$	$= 7.421 \mu\text{m}^2/\text{kg}$
$C_2$	$= 41.04 \mu\text{m}^2/\text{kg}$

(a)



(b)

Fig. 5.1: (a) Cross section of a circular core fiber, (b) Comparison of thermal stress obtained from analytical method and the FEM.

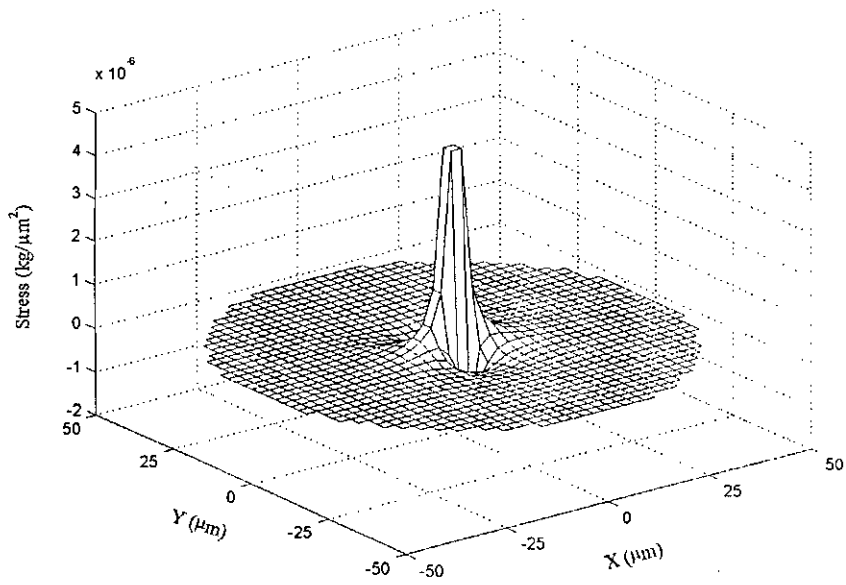


Fig. 5.2: Stress ( $\sigma_x$ ) distribution over the cross section of circular fiber.

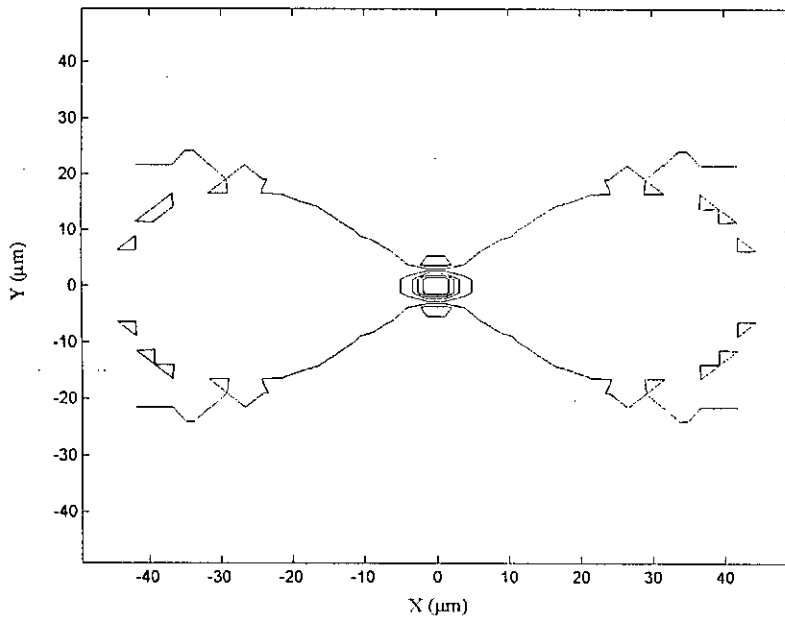


Fig. 5.3: Contour map corresponding to Fig. 5.2.

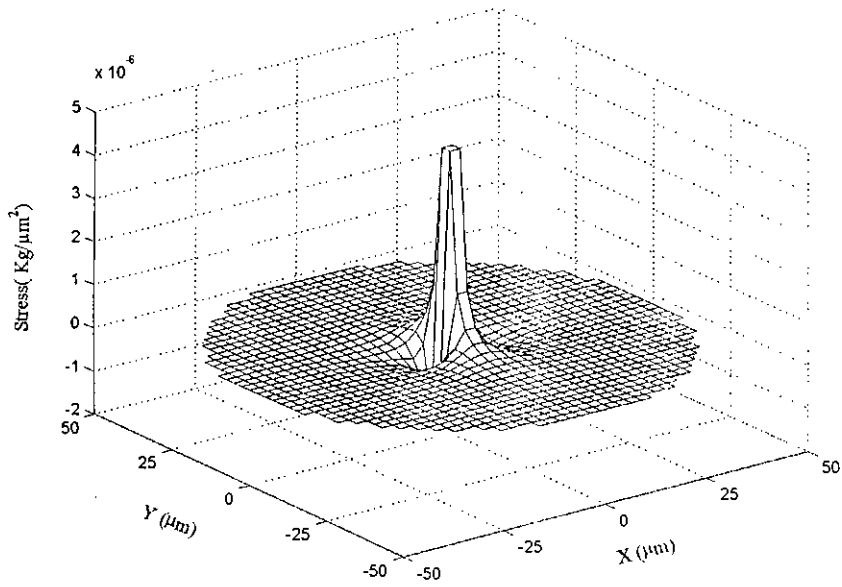


Fig. 5.4: Stress ( $\sigma_y$ ) distribution over the cross section of circular fiber.

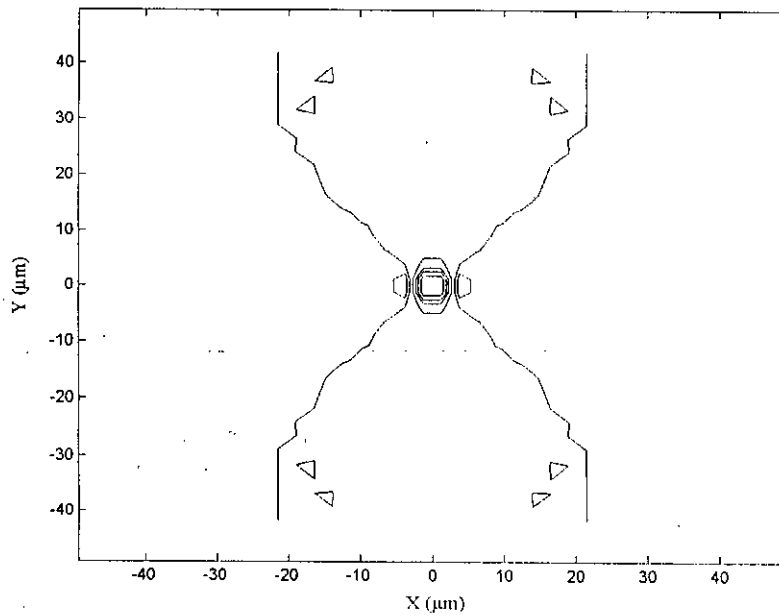


Fig. 5.5: Contour map corresponding to Fig. 5.4.

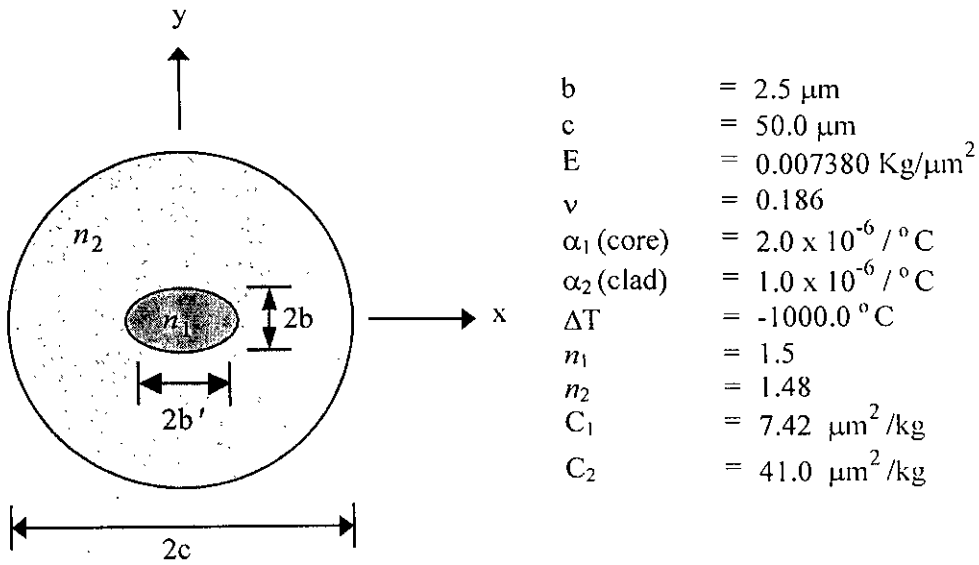


Fig. 5.6: Cross section of an elliptical core fiber.

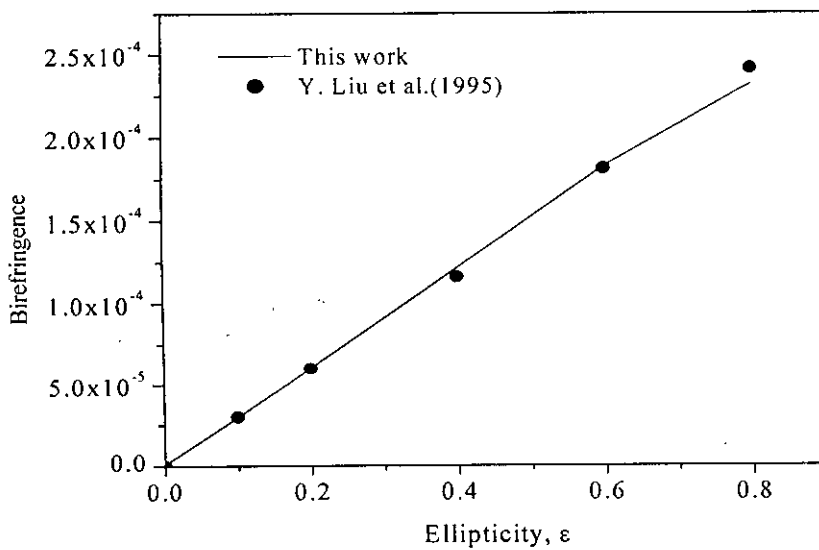


Fig. 5.7: Variation of birefringence with core ellipticity.

In Fig. 5.6, an optical fiber with elliptical core is considered. We calculated the birefringence using (4.33), where the new refractive indices as obtained considering the elasto-optic effect due to thermal stress are used. In Fig. 5.7, the calculated

birefringence versus core ellipticity is shown. The results are compared with the results of Liu et al. (1995) [7]. The solid line shows our result and the dark circles show the results of Y. Liu et al. (1995) [7]. The results agreed very well. It is seen that the fiber birefringence increases with the core ellipticity. This is due to the increased difference of refractive indices in  $x$  and  $y$  directions. It can be seen in the numerical results that due to elasto-optic effect of thermal stress, the change in the index value of  $x$  direction ( $\Delta n_x$ ) is greater than the change in the index of  $y$  direction ( $\Delta n_y$ ) when ellipticity increases. As a consequence, the birefringence increases with the increase in ellipticity. The stress distributions are shown in Figs. 5.8, 5.9, 5.10, 5.11 for ellipticity,  $\varepsilon = 0.6$ . It is observed that the high stress is concentrated over the core region of the fiber. As the core ellipticity changes the nature of high stress changes accordingly. The increase of core ellipticity means the increase of core region in  $x$  direction, which produces higher degree of asymmetry and hence greater stress. The maximum value of the  $x$  component of thermal stress for elliptical core fiber with ellipticity 0.0 (i.e circular core), 0.2 and 0.6 were found to be  $4.6 \times 10^{-6}$ ,  $5.46 \times 10^{-6}$  and  $7.26 \times 10^{-6}$  kg/ $\mu\text{m}^2$ . This indicates that thermal stress increases with ellipticity. For the  $y$  component ( $\sigma_y$ ) of stress distribution we get the noticeable negative value, which increases negatively with core ellipticity. Because of all these, the birefringence increases with the increase in ellipticity.

In Fig. 5.12 and Fig. 5.13, the change in refractive indices due to thermal stress are shown for elliptical core fiber with  $\varepsilon = 0.6$ . From these figures it is clear that the change of refractive index from unstressed to thermal stress condition has a profound effect over the core region and elsewhere it is negligible.

Next, we consider side-hole optical fiber and investigate the effect of air hole placed on each side of  $x$ - direction in an elliptical core fiber. The influence of pitch length (i.e the distance between core center and side-hole center), side-hole radius and position on fiber birefringence will be examined. The birefringence variations due to temperature change during fiber manufacturing and thermal expansion coefficient of core and cladding materials will also be investigated. The fiber structure and parametric values are depicted in Fig. 5.14.

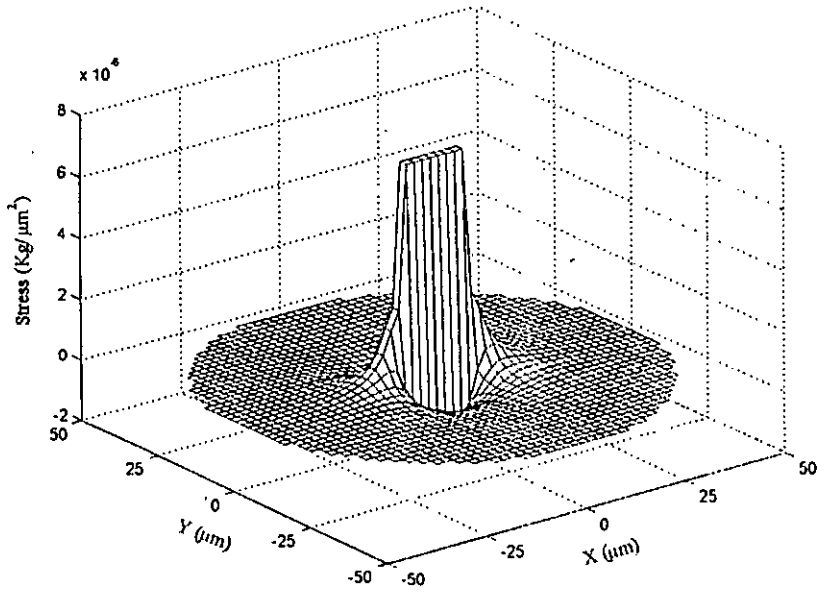


Fig. 5.8: Stress ( $\sigma_x$ ) distribution over the cross section of elliptical core ( $\epsilon = 0.6$ ) fiber.

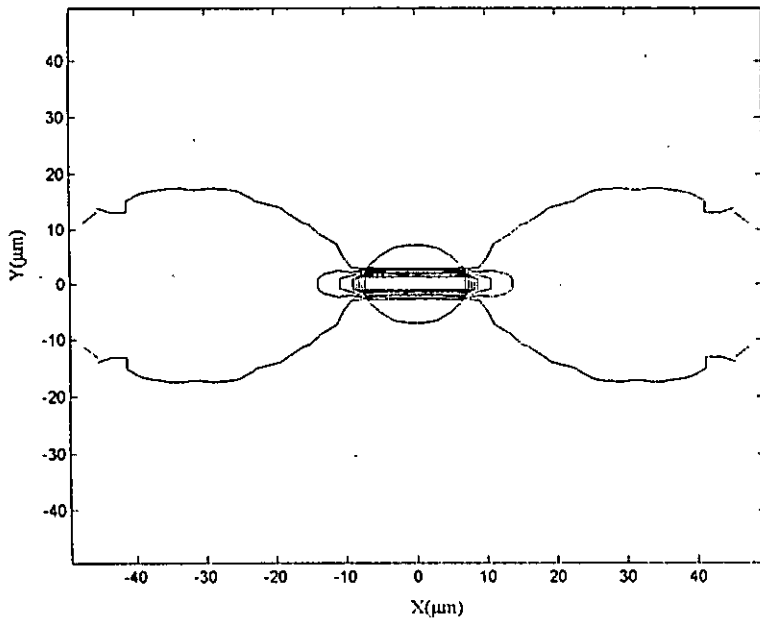


Fig. 5.9: Contour map corresponding to Fig. 5.8

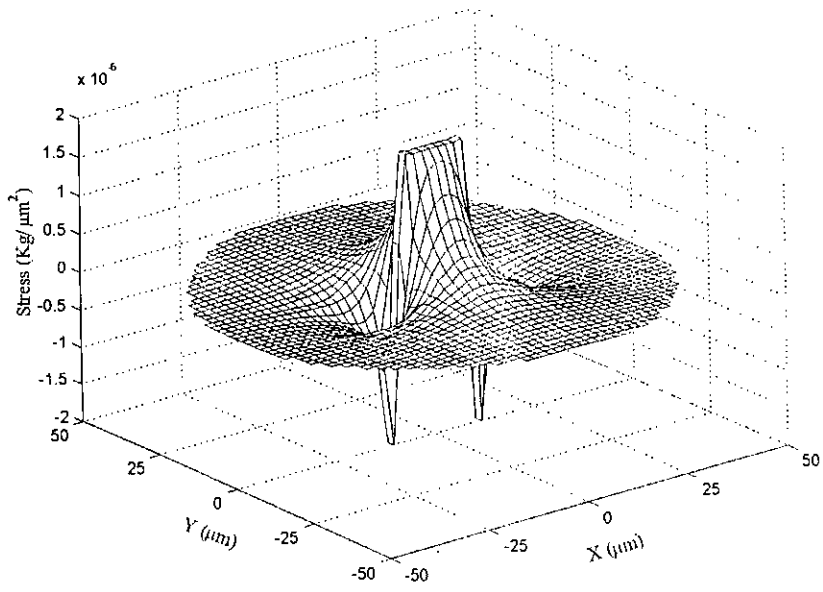


Fig. 5.10: Stress ( $\sigma_y$ ) distribution over the cross section of elliptical core ( $\epsilon = 0.6$ ) fiber.

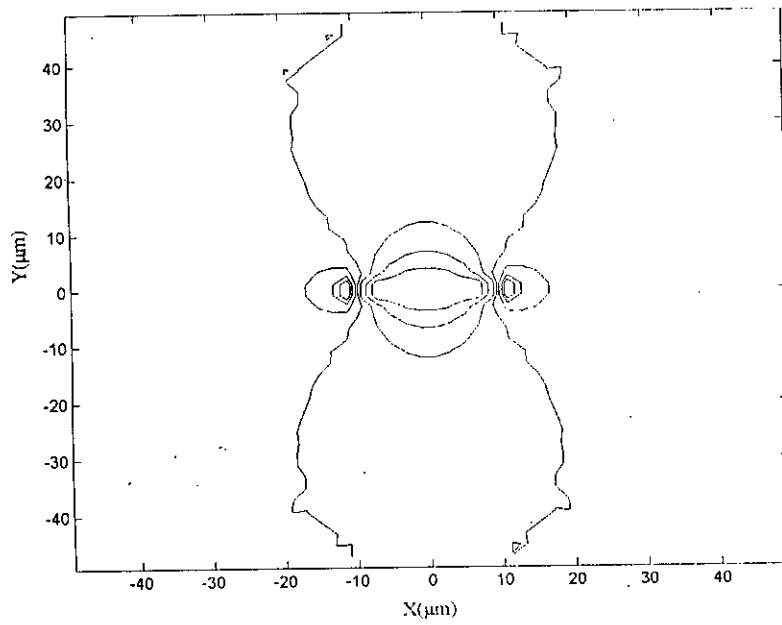


Fig. 5.11: Contour map corresponding to Fig. 5.10



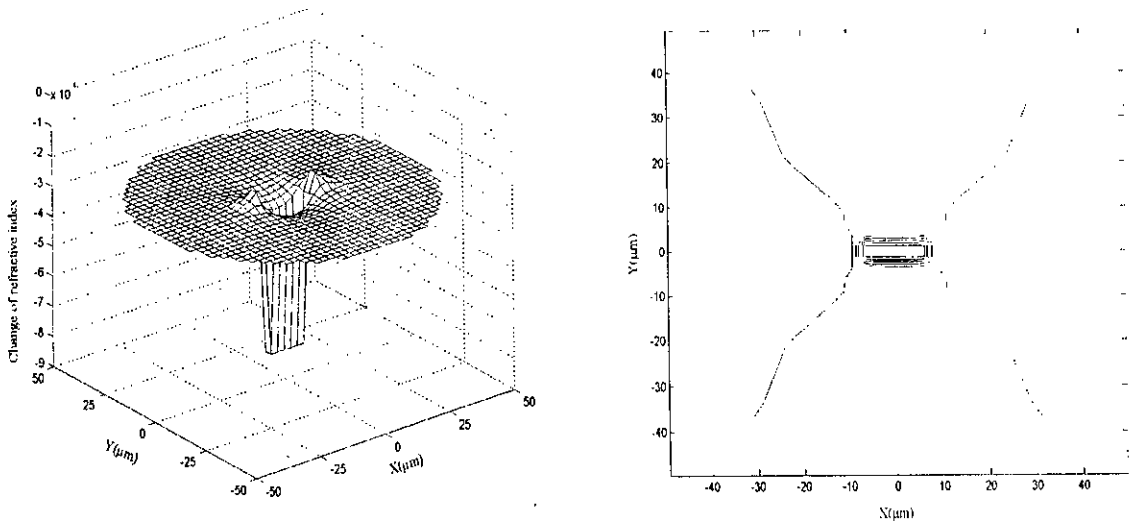


Fig. 5.12: Refractive index difference ( $\Delta n_x$ ) and the corresponding contour map over the cross section of elliptical core ( $\epsilon = 0.6$ ) fiber.

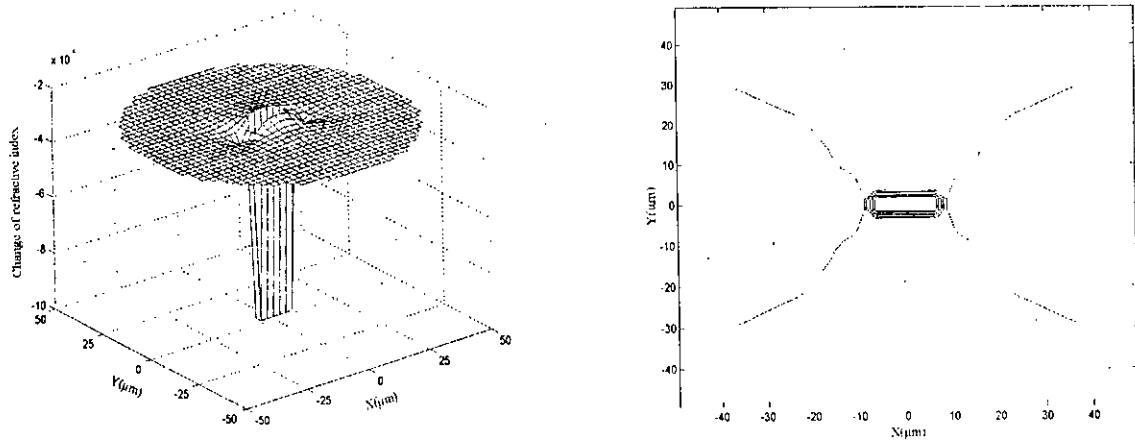
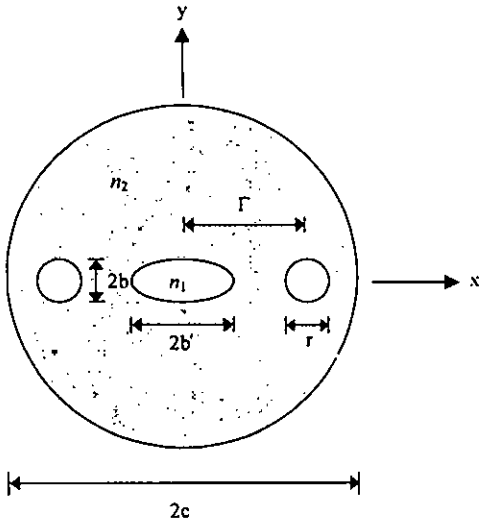


Fig. 5.13: Refractive index difference ( $\Delta n_y$ ) and the corresponding contour map over the cross section of elliptical core ( $\epsilon = 0.6$ ) fiber.

5.3 Results of Side-hole Fiber with Elliptical Core



- b = 2.5 μm
- c = 50.0 μm
- E = 0.007380 Kg/μm<sup>2</sup>
- ν = 0.186
- α<sub>1</sub> (core) = 2.0 x 10<sup>-6</sup> / °C
- α<sub>2</sub> (clad) = 1.0 x 10<sup>-6</sup> / °C
- ΔT = -1000.0 °C
- n<sub>1</sub> = 1.45
- n<sub>2</sub> = 1.435
- C<sub>1</sub> = 7.42 μm<sup>2</sup>/kg
- C<sub>2</sub> = 41.0 μm<sup>2</sup>/kg
- Side hole radius, r = 7.5 μm
- and, Γ = Pitch length

Fig. 5.14: Cross section of the side-hole fiber with elliptical core.

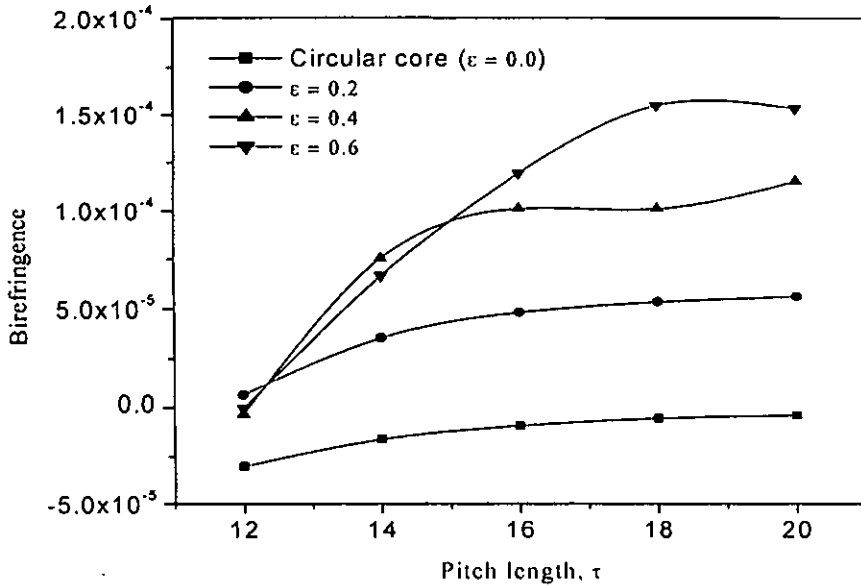


Fig. 5.15: Birefringence versus pitch length of side-hole fiber.

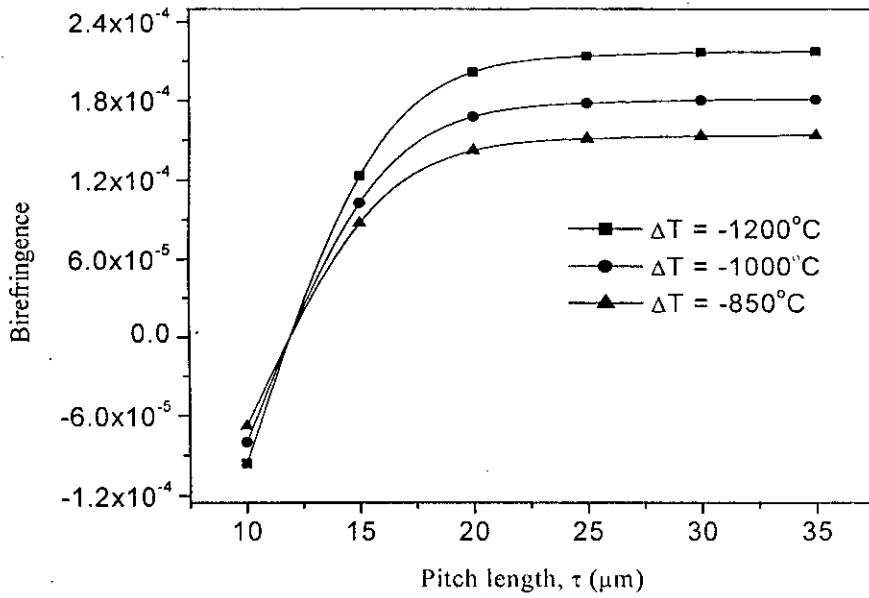


Fig. 5.16: Birefringence versus pitch length when core ellipticity,  $\varepsilon = 0.6$ .

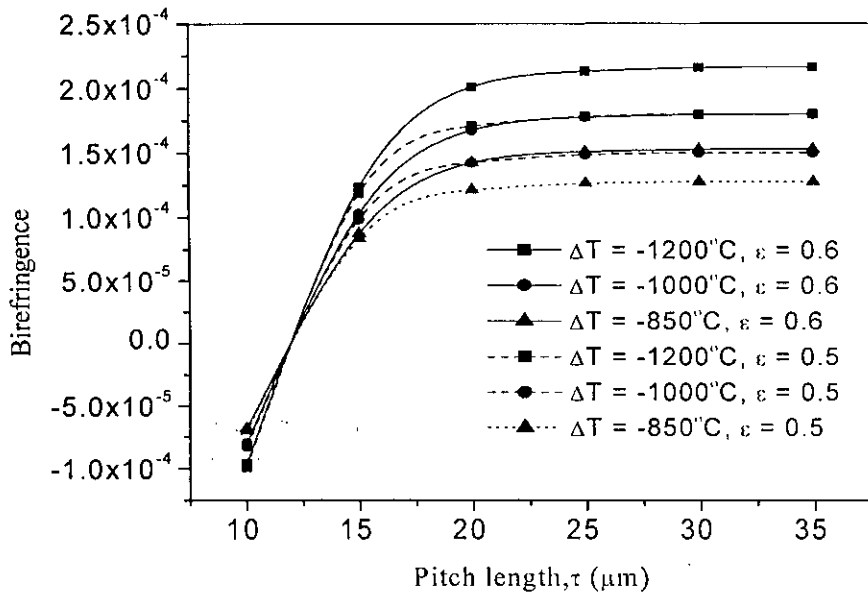


Fig. 5.17: Birefringence versus pitch length with core ellipticity,  $\varepsilon = 0.6$  and  $0.5$ .

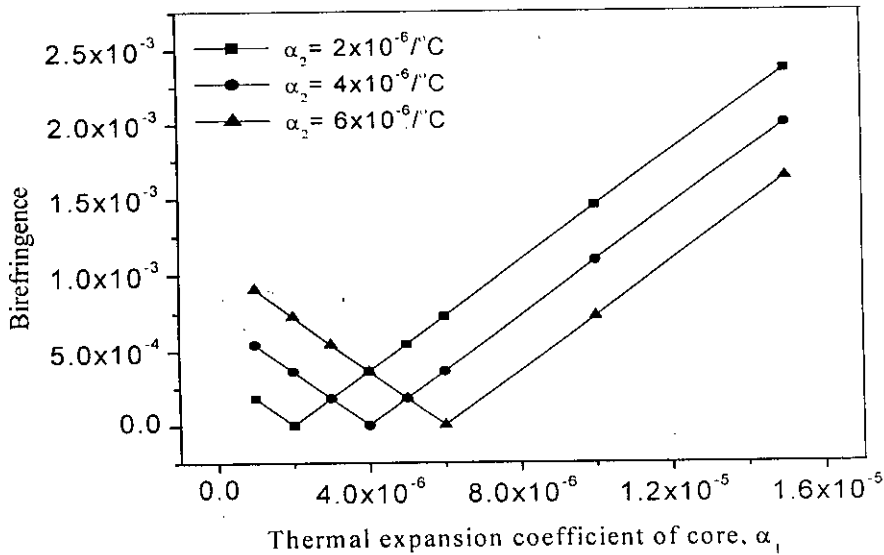


Fig 5.18: The birefringence versus thermal expansion co-efficient of fiber core material.

Fig. 5.15 shows the effect of pitch length on birefringence of a side hole fiber with air hole radius,  $r = 7.5 \mu\text{m}$ . The higher the pitch length the greater birefringence is obtained. Here we have four curves; one for circular core and three for elliptical core ( $\varepsilon = 0.2$ ,  $\varepsilon = 0.4$ ,  $\varepsilon = 0.6$ ) fibers, among which  $\varepsilon = 0.6$  is on the top. It has birefringence of  $1.709 \times 10^{-4}$  at  $\tau = 20.0 \mu\text{m}$ . On the bottom, the circular core fiber produce  $-4.203 \times 10^{-6}$  birefringence at  $\tau = 20.0 \mu\text{m}$ . So the fiber with core ellipticity,  $\varepsilon = 0.6$  and greater pitch length will generate high birefringence.

Fig. 5.16 and 5.17 show the variation of birefringence on pitch length and ellipticity . These figures also show the effect of change of temperature. It can be seen that the higher ellipticity and temperature change result greater birefringence at larger pitch length.

Fig. 5.18 shows the birefringence dependence on the thermal expansion coefficient of core material ( $\alpha_1$ ) for three values of the thermal expansion coefficient of cladding material  $\alpha_2 = (2, 4, 6) \times 10^{-6} / ^\circ\text{C}$ . From this figure it can be seen that for each

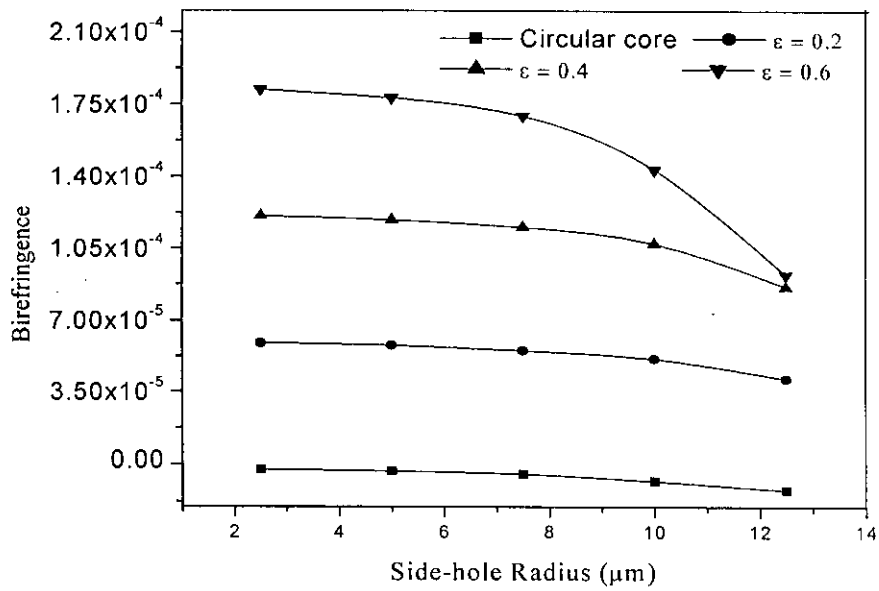


Fig. 5.19: Birefringence versus air hole radius for a pitch length,  $\Gamma = 20.0 \mu\text{m}$ .

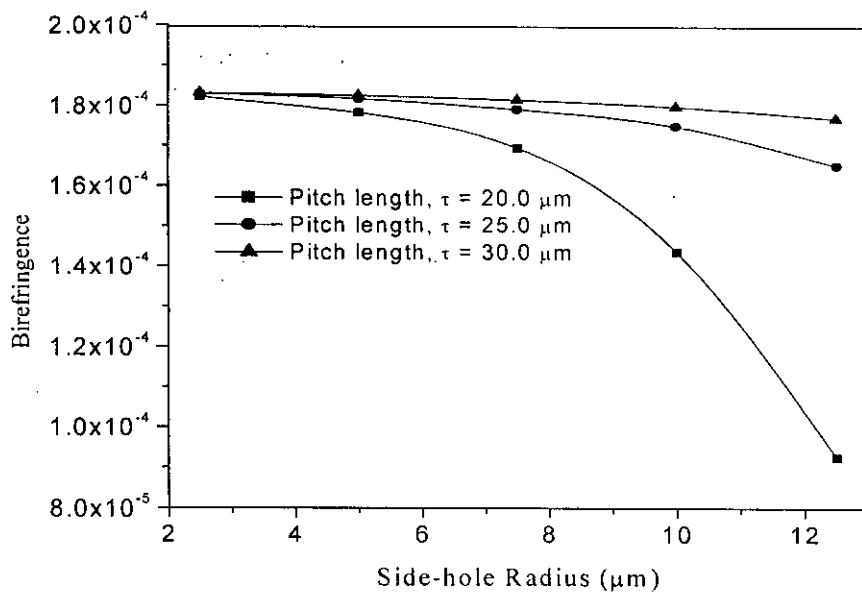


Fig. 5.20: Birefringence versus air-hole radius for different pitch length when core ellipticity,  $\epsilon = 0.6$

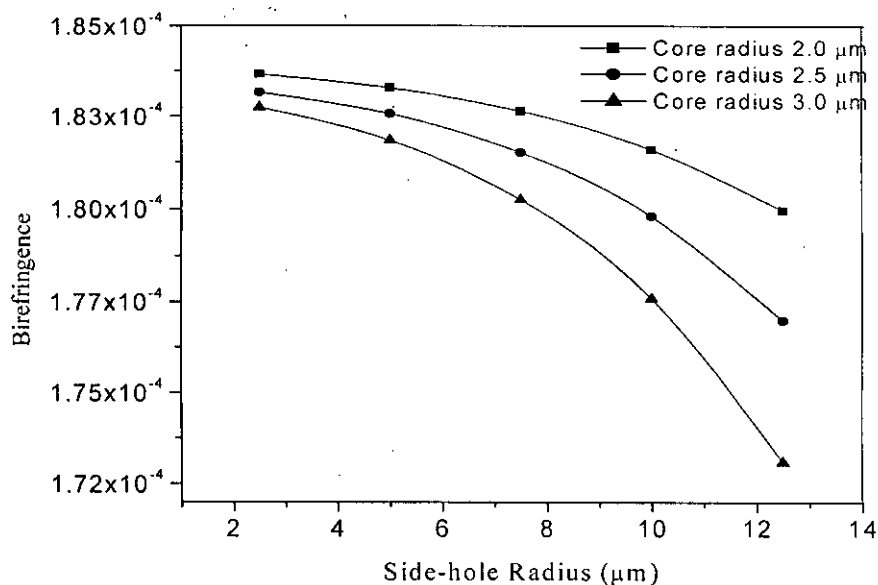


Fig. 5.21: Birefringence versus air-hole radius for different core radius with pitch length 30 μm and core ellipticity 0.6.

curve, the fiber birefringence decreases linearly, when  $\alpha_1$  is less than  $\alpha_2$  and it increases linearly, when  $\alpha_1$  is greater than  $\alpha_2$  resulting absolute zero value of birefringence at  $\alpha_1 = \alpha_2$ .

In Fig 5.19 the birefringence versus side hole radius is shown. We calculated birefringence for four fibers; one for circular core and three for elliptical core ( $\epsilon = 0.2$ ,  $\epsilon = 0.4$  and  $\epsilon = 0.6$ ) fiber. We found largest birefringence  $1.8226 \times 10^{-4}$  for  $\epsilon = 0.6$  with side hole radius 2.5 μm. Whereas, circular fiber produces lowest birefringence -  $1.2179 \times 10^{-5}$  with side hole radius 12.5 μm. So, birefringence decreases with the increase of side hole radius.

As it is found that a fiber with  $\epsilon = 0.6$  producing highest birefringence, we calculated birefringence with various side hole radius at different pitch length and the results are shown in Fig. 5.20. A smaller side hole at far away from the core generates higher birefringence in this case. The value of the birefringence is  $1.8258 \times 10^{-4}$  for side hole radius 5.0 μm and a pitch length 30.0 μm.

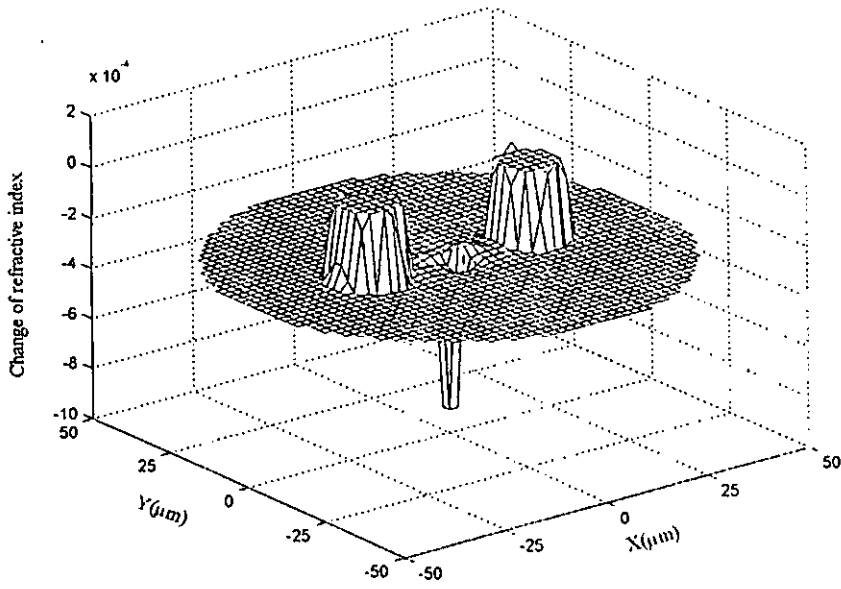


Fig. 5.22: Change of refractive index ( $n_x$ ) over the cross section for circular core side hole fiber with  $\Gamma = 20.0 \mu\text{m}$  and  $r = 7.5 \mu\text{m}$ .

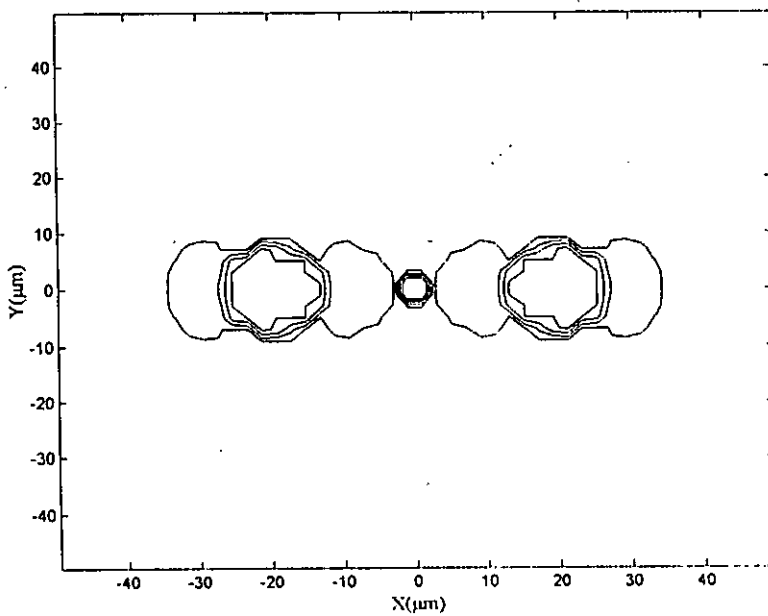


Fig. 5.23: Contour map corresponding to Fig.5.22.

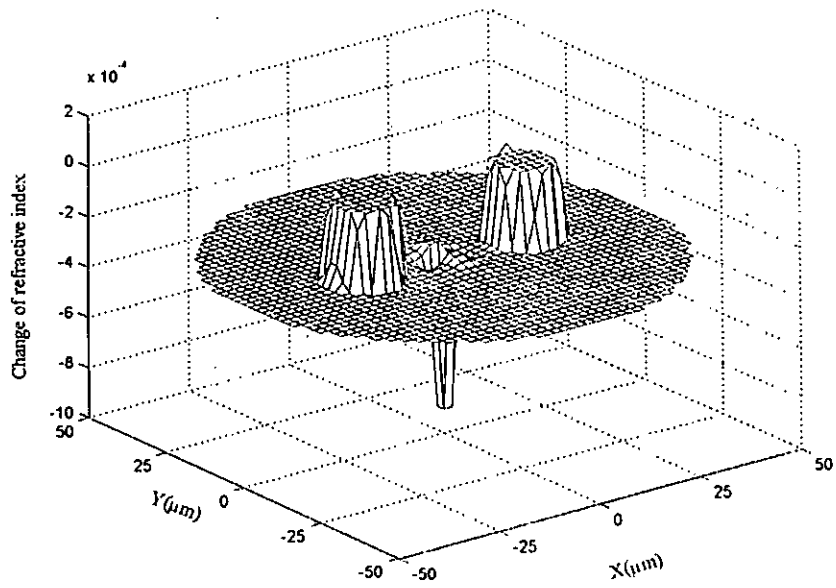


Fig. 5.24: Change of refractive index ( $n_y$ ) over the cross section for circular core side hole fiber with  $\Gamma = 20.0 \mu\text{m}$  and  $r = 7.5 \mu\text{m}$ .

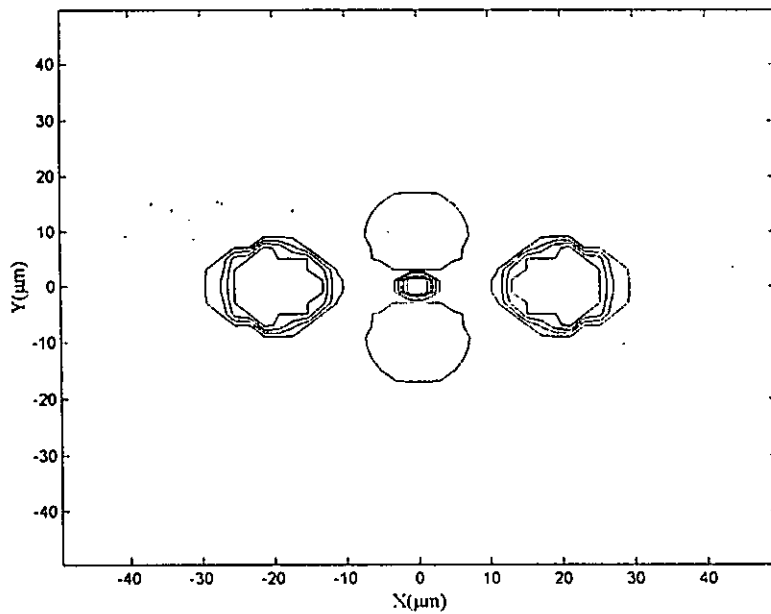


Fig. 5.25: Contour map corresponding to Fig. 5.24.



In Fig. 5.21 birefringence curves for different core radius and side hole radius are shown to evaluate the effect of core size. From the figure it is clear that fiber with smaller core and side hole radius produce higher birefringence. To illustrate the effect of thermal stress on side hole fiber, finally we show the change of refractive index over the cross section of the fiber in Fig. 5.22 through Fig. 5.25. Although the refractive index changes all over the cross section except the air hole area, the change is significant in the core and around the air holes. These changes may affect the optical behaviour of the fiber, such as its cut-off wavelength. So, it has to be taken into account very carefully.

## Chapter 6

# Conclusions

### 6.1 Summary of the work

In this work, the thermal stress analysis of optical fiber is carried out by using finite element method. The stress analysis is based on the plain strain approximation and potential energy principle, which finally results in a linear system of unknown displacements caused by thermal strain. Here, one-fourth of the fiber cross section is divided into finite number of linear triangular elements and Dirichlet type boundary conditions are applied to obtain the final system of equations. The Gaussian elimination technique is then employed for solving the system of equations to obtain the nodal displacements. Elemental stress is then calculated from the elemental nodal displacements. The program is further extended to calculate the changed refractive index in  $x$  and  $y$  polarized light using photo-elastic coefficient and hence the birefringence of the fiber is calculated.

At first, the program is verified for a simple circular fiber structure with circular core by comparing the solutions with the exact analytical solutions of stress. Then the birefringence for non-circular core fiber is calculated and compared with the existing published results. For elliptical core fiber, the birefringence increases with the core ellipticity. The stress in and around the core gets higher with the increase in the core ellipticity.

The developed system is then applied for the analysis of side-hole fiber with elliptical core. The stress in this case will be developed in the core and also in the cladding just around the air holes.

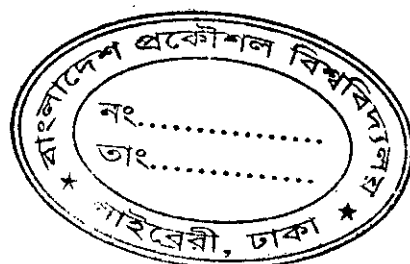
It is found that fiber with higher core ellipticity and larger pitch length generates higher birefringence. Increased difference of refractive indices in  $x$  and  $y$  directions is responsible for the higher birefringence.

We found that the fiber birefringence increases with greater change of temperature during the fiber manufacturing process. At the same time, thermal expansion coefficients of core and cladding materials have profound effect on birefringence.

Fiber birefringence decreases with increase in side-hole radius when the pitch length is kept constant. On the other hand, smaller side-holes far from the core generate higher birefringence. Fiber with smaller core and side holes also can produce higher birefringence. So, fiber with elliptical core and smaller side-hole radius far from core center (longer pitch length) can be used as a good member of polarization maintaining fiber.

## 6.2 Future research scope

In this work, only two air holes on each side of fiber core is considered. Therefore, a future work can be done with more than two air holes in different arrangements. The developed simulation program can be extended to study the variation of birefringence for fibers with air holes circularly around the core. Air holes in two layers can also be considered. We examined only the birefringence property of fiber due to thermal stress and geometry of the core. However, modal analysis and calculation of other fiber characteristics like dispersion and loss of different polarization maintaining fiber can be another suggestion for future research work. Most importantly, the system can be extended for the analysis of photonic crystal fibers under stress as well.



# References

- [1] J. Noda, K. Okamoto, and Y. Sasaki, "Polarization-Maintaining Fibers and Their Applications," *IEEE J. Lightwave Technol.*, vol. LT-4, no. 8, pp. 1071-1089, Aug. 1986.
- [2] J. Sakai and T. Kimura, "Birefringence Caused by Thermal Stress in Elliptically Deformed Core Optical Fibers," *IEEE J. Quantum Electron.*, vol. QE-18, no. 11, pp. 1899-1909, Nov. 1982.
- [3] W. Urbanczyk, T. Martynkien, and W. J. Bock, "Dispersion effects in elliptical-core highly birefringent fibers," *Appl. Optics.*, vol. 40, no. 12, pp. 1911-1920, Apr. 2001.
- [4] I. Hwang, Y. Lee, K. Oh, and D. N. Payne, "High birefringence in elliptical hollow optical fiber," *Optics Express*, vol. 12, no. 9, pp. 1916-1923, May 2004.
- [5] H. M. Xie, Ph. Dabkiewicz, and R. Ulrich, "Side-hole fiber for fiber-optic pressure sensing," *Optics Lett.*, vol. 11, no. 5, pp. 333-335, May 1996.
- [6] J. R. Clowes, S. Syngellakis, and M. N. Zervas, "Pressure Sensitivity of Side-Hole Optical Fiber Sensors," *IEEE Photon. Technol. Lett.*, vol. 10, no. 6, pp. 857-859, June 1998.
- [7] Y. Liu, B.M.A. Rahman, and K.T.V. Grattan, "Analysis of the Birefringence Properties of Optical Fibers Made by a Preform Deformation Technique," *IEEE J. Lightwave Technol.*, vol. 13, no. 2, pp. 142-147, Feb. 1995.
- [8] K. Okamoto, *Fundamentals of Optical Waveguides*, Academic Press, 2000.

- [9] T. Schreiber, H. Schultz, O. Schmidt, F. Röser, J. Limpert, and A. Tünnermann, "Stress-induced birefringence in large-mode-area micro-structured optical fibers," *Optics Express*, vol. 13, no. 10, pp. 3637-3645, May 2005.
- [10] T. Okoshi, K. Oyamada, M. Nishimura, and H. Yokota, "Side-tunnel fiber: an approach to polarization-maintaining optical waveguiding scheme," *Electron Lett.*, vol. 18, pp. 824-826, 1982.
- [11] T. Okoshi, T. Aihara, and K. Kikuchi, "Prediction of ultimate performance of sidetunnel single-polarization fiber," *Electron. Lett.*, vol. 19, pp. 1980-1982, 1983.
- [12] K. Hayata, M. Eguchi, M. Kshiba, and M. Suzuki, "Vectorial wave-analysis of sidetunnel type polarization-maintaining optical fibers by variational finite elements," *IEEE J. Lightwave Technol.*, vol. LT-4, pp. 1090-1096, 1986.
- [13] A. N. Kaul, A. Kumar, and K. Thyagarajan, "Polarization characteristics of side-pit and side-tunnel fibers using the effective index method," *IEEE J. Lightwave Technol.*, vol. LT-5, pp. 1610-1612, 1987.
- [14] T. Hosaka, K. Okamoto, Y. Sasaki, and T. Edahiro, "Single mode fibers with asymmetrical refractive index pits on both sides of core," *Electron. Lett.*, vol. 17, pp. 191-193, 1981.
- [15] K. Okamoto, T. Hosaka, and T. Edahiro, "Stress analysis of optical fibers by a finite element method," *IEEE J. Quantum Electron.*, QE-17, pp. 2123-2129, Oct. 1981.
- [16] M. P. Varnham, D. N. Payne, A. J. Barlow, and R. D. Birch, "Analytic solution for the birefringence produced by thermal stress in polarisation-maintaining optical fibers," *IEEE J. Lightwave Technol.*, vol. LT-1, pp. 332-3329, 1983.
- [17] P. L. Chu, and R. A. Sammut, "Analytical method for calculation of stresses and material birefringence in polarisation maintaining optical fiber," *IEEE J. Lightwave*

*Technol.*, vol. LT-2, pp. 650-662, 1984.

[18] M. Born and E. Wolf, *Principles of Optics*, Pergamon Press, Sixth ed. 1988.

[19] J. M. Senior, *Optical Fiber Communication-principles and practice*. India: Prentice Hall, Second ed., 2003.

[20] G. P. Agrawal, *Fiber Optic Communication Systems*. New York: Wiley, 1992.

[21] G. Keiser, *Optical Fiber Communications*. New York: Mc Graw-Hill Engineering, Third ed., 2001.

[22] I. P. Kaminow, "Polarization in optical fibers," *IEEE J. Quantum Electron.*, vol. QE-17, pp. 15-22, 1981.

[23] T. Okoshi, "Polarization phenomena in optical fibers," *Optical Fiber Sensors Proceedings of The NATO Advanced Study Institute*, pp. 227-242, 1987.

[24] E. Sasaoka, M. Takagi, H. Suganuma, Y. Kubo, S. Tanaka, and H. Yokota, "Polarization maintaining optical fiber and components," *Sumitomo Electric Technical Review*, no. 35, pp. 29-33, 1993.

[25] S. B. Poole, and D. N. Payne, "Special optical fibers," *SPIE, Fiber Optics '87: Fifth International Conference on Fiber Optics and opto-Electronics*, pp. 92-103, 1987.

[26] T. Okoshi, and K. Oyamada, "Single-polarization single-mode optical fiber with refractive-index pits on both sides of core," *Electron. Lett.*, vol. 16, pp. 712-713, 1980.

[27] Y. Liu, B. M. A Rahman, and T. V. Grattan, "Thermal-stress-induced birefringence in bow-tie optical fibers," *Appl. Opt.*, vol. 33, no. 24, 20 August 1994.

- [28] R. D. Birch, D. N. Payne, and M. P. Varnham, "Fabrication of polarization maintaining fibers using gas-phase etching," *Electron. Lett.*, vol. 18, pp. 1036-1038, 1982.
- [29] Y. Sasaki, K. Okamoto, T. Hosaka, and N. Shibata, "polarization-maintaining and absorption reducing fibers," *Tech. Dig. Topical Meeting Opt. Fiber Commun., Phoenix AZ*, 1982.
- [30] R. B. Dyott, J. R. Cozens, and D. G. Morris, "Preservation of polarization in optical fiber waveguides with elliptical cores," *Electron. Lett.*, vol. 15, pp. 380-382, 1979.
- [31] T. Katuyama, H. Matsumura, and T. Suganuma, "Low-loss single-polarization fibers," *Electron. Lett.*, vol. 17, pp. 473-474, 1981.
- [32] J. Jin, *The Finite Element Method for Electromagnetics*, John Wiley & Sons, Inc., 1993.
- [33] O.C Zienkiewicz, *The Finite Element Method in Engineering Science*, New York: Mc Graw-Hill, 1971.
- [34] E. Hinton and D.R.J Owen, *Finite Element Programming*, Academic Press, Inc. (London), 1977.

